pubs.acs.org/acschemicalbiology

Articles

Translesion Synthesis across the N^2-Ethyl-deoxyguanosine Adduct by Human PrimPol

Elizaveta O. Boldinova,[§] Pratibha P. Ghodke,[§] Sruthi Sudhakar,[§] Vipin Kumar Mishra, Anna A. Manukyan, Nataliya Miropolskaya, Pushpangadan I. Pradeepkumar,* and Alena V. Makarova*

Cite This: *ACS Chem. Biol.* 2022, 17, 3238−3250

Read Online

ACCESS | Metrics & More | Article Recommendations | Supporting Information

ABSTRACT: Primase-DNA polymerase (PrimPol) is involved in reinitiating DNA synthesis at stalled replication forks. PrimPol also possesses DNA translesion (TLS) activity and bypasses several endogenous nonbulky DNA lesions in vitro. Little is known about the TLS activity of PrimPol across bulky carcinogenic adducts. We analyzed the DNA polymerase activity of human PrimPol on DNA templates with seven N^2-dG lesions of different steric bulkiness. In the presence of Mg^{2+} ions, bulky N^2-isobutyl-dG, N^2-benzyl-dG, N^2-methyl(1-naphthyl)-dG, N^2-methyl(9-anthracenyl)-dG, N^2-methyl(1-pyrenyl)-dG, and N^2-methyl(1,3-dimethoxyanthraquinone)-dG adducts fully blocked PrimPol activity. At the same time, PrimPol incorporated complementary deoxycytidine monophosphate (dCMP) opposite N^2-ethyl-dG with moderate efficiency but did not extend DNA beyond the lesion. We also demonstrated that mutation of the Arg288 residue abrogated dCMP incorporation opposite the lesion in the presence of Mn^{2+} ions. When Mn^{2+} replaced Mg^{2+}, PrimPol carried out DNA synthesis on all DNA templates with N^2-dG adducts in standing start reactions with low efficiency and accuracy, possibly utilizing a lesion "skipping" mechanism. The TLS activity of PrimPol opposite N^2-ethyl-dG but not bulkier adducts was stimulated by accessory proteins, polymerase delta-interacting protein 2 (PolDIP2), and replication protein A (RPA). Molecular dynamics studies demonstrated the absence of stable interactions with deoxycytidine triphosphate (dCTP), large reactions, and C1′−C1′ distances for the N^2-isobutyl-dG and N^2-benzyl-dG PrimPol complexes, suggesting that the size of the adduct is a limiting factor for efficient TLS across minor groove adducts by PrimPol.

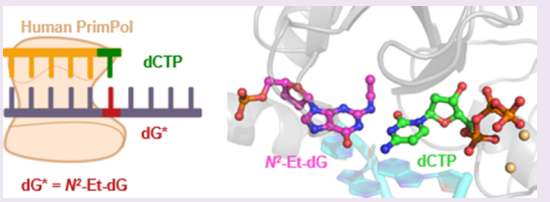

INTRODUCTION

Human primase-DNA polymerase (PrimPol) belongs to the archaea-eukaryotic primase (AEP) superfamily and possesses DNA primase and DNA polymerase activities.[1,2] The principal role of PrimPol is believed to be the reinitiation of DNA synthesis de novo at stalled replication forks on sites of DNA damage (such as abasic sites and photoproducts) and non-B DNA structures in nuclei and mitochondria.[3−8] In particular, PrimPol plays a role in DNA damage tolerance to bulky benzo[*a*]pyrene diol epoxide adducts by re-priming and forming postreplicative gaps, which can be repaired by homologous recombination.[9] While acting as a DNA damage tolerance primase during DNA synthesis, PrimPol might encounter DNA lesions.

Several in vitro studies showed that PrimPol could act as a polymerase replicating across DNA lesions. PrimPol effectively incorporates deoxyribonucleoside monophosphate (dNMP) opposite nonbulky DNA lesions such as 8-oxoguanine (8-oxo-G),[1,2,10,11] O^6-methylguanine, and 5-formyluracil.[11] PrimPol also bypasses an abasic site and T−T (6−4) photoproducts using a lesion "skipping" mechanism (also called the "template scrunching" mechanism).[1,3,11,12] At the same time, PrimPol is blocked opposite N^6-ethenoadenine and thymine glycol lesions.[2,11] Little is known about the behavior and TLS activity of PrimPol on DNA with bulky carcinogenic minor groove adducts.

The exocyclic N^2-atom of guanine is well known to form stable DNA adducts upon reactions with multiple carcinogenic agents from the metabolites of aromatic amines, polycyclic aromatic hydrocarbons,[13−15] and aldehydes.[16] N^2-dG adducts protrude in the minor groove of DNA.[17−20] Since the interaction of DNA polymerases with the minor groove of DNA is essential for its activity, N^2-dG adducts, depending on their size and shape, can disrupt contacts of DNA polymerases with DNA and block the replication.[17,21−23] Many unrepaired bulky N^2-dG adducts present a strong block to high-fidelity replicative DNA polymerases.[21,22] In contrast, a few DNA polymerases (e.g., Pol κ, Pol η, and Pol ι) efficiently bypass N^2-dG adducts in vitro[22,24−27] via TLS DNA synthesis. In this work, we analyzed the DNA polymerase activity of PrimPol

Received: September 19, 2022
Accepted: October 11, 2022
Published: November 1, 2022

https://doi.org/10.1021/acschembio.2c00717
ACS Chem. Biol. 2022, 17, 3238−3250

on DNA templates with seven N^2-dG lesions of varying steric bulkiness and chemical nature (Figure 1).

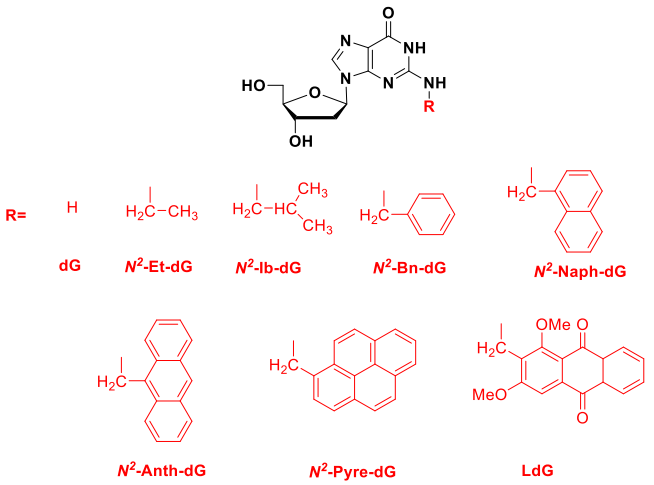

Figure 1. Structures of N^2-dG adducts used in this study.

The N^2-ethyl-dG (N^2-Et-dG) adduct is one of the DNA modifications produced by acetaldehyde.[28] Sources of acetaldehyde in the environment are multiple and diverse, and they include products of tobacco burning, coffee roasting, alcohol beverage consumption, fuel combustion, coal refining, and waste processing.[29−31] The reaction of acetaldehyde with the exocyclic amino group of guanosine results in the formation of the unstable N^2-ethylidenedeoxyguanosine adduct following reduction by glutathione or ascorbic acid to form a stable N^2-Et-dG lesion.[32]

Many studied bulky N^2-dG adducts are environmental carcinogens. N^2-benzyl-dG (N^2-Bn-dG) is formed by DNA benzylating species metabolized from *N*-nitroso-*N*-benzylurea,[33] *N*-nitrosobenzylmethylamine,[34] and benzyl halides,[35] and is detected in vivo in lung and liver DNA.[33] N^2-methyl(1,3-dimethoxyanthraquinone)-dG (LG) adduct is formed by lucidin and rubaidin molecules metabolized from carcinogenic hydroxyantharaquinones and their glycoside conjugates derived from a medicinal plant*Rubia tinctorum*L.[36] N^2-methyl(1-pyrenyl)-dG (N^2-Pyre-dG) was detected in liver, kidney, and lung DNA of mice exposed to carcinogens 1-methylpyrene[37] and 1-hydroxymethyl-pyrene.[38] N^2-methyl(9-anthracenyl)-dG (N^2-Anth-dG) is a product of the reaction of DNA with 9-(sulfoxymethyl)-anthracene, an electrophilic metabolite of carcinogenic 9-hydroxymethyl-anthracene.[39] However, N^2-isobutyl-dG (N^2-Ib-dG) and N^2-methyl(1-naphthyl)-dG (N^2-Naph-dG) are yet to be found in vivo.

PrimPol was shown to be more active in the presence of Mn^{2+} ions, compared to Mg^{2+}.[1,40] The Glu116 residue of the PrimPol active site favors the use of Mn^{2+} ions and is required for optimal incoming nucleotide stabilization.[40] Mn^{2+} ions stimulate the TLS activity of PrimPol on DNA with many lesions including an 1,2-intrastrand cisplatin cross-link and photoproducts but reduce the accuracy of nucleotide incorporation.[9,41] Herein, the TLS activity of PrimPol was tested in the presence of Mg^{2+} and Mn^{2+} ions and accessory proteins, polymerase delta-interacting protein 2 (PolDIP2) and replication protein A (RPA).

MATERIALS AND METHODS

Proteins. The wild-type PrimPol and its R47A and R76A mutant variants were purified from the Rosetta 2 strain of *Escherichia coli* as described earlier.[42,43] Mutations encoding the R288A and N289A amino acid substitutions were introduced in the *PRIMPOL* gene by site-directed mutagenesis, and the corresponding proteins were purified as the wild-type enzyme. Yeast Pol ζ_4, PolDIP2, and RPA were purified as reported earlier.[44−46]

DNA Adducts and Oligonucleotide Substrates. All the modified oligonucleotide substrates, the corresponding undamaged DNA template, and primers were synthesized as described.[17,47] The purity of oligonucleotides was confirmed by matrix-assisted laser desorption/ionization (MALDI)/electrospray ionization (ESI) spectrometry. The structures of DNA adducts are presented in Figure 1.

To obtain DNA substrates for the primer extension reactions, the 15-mer and 11-mer primers were 5′-labeled with [γ-^{32}P]-ATP by T4 polynucleotide kinase (SibEnzyme) and annealed to the corresponding unlabeled 50-mer template at a molar ratio of 1:1.1 (primer:template). DNA substrates were heated at 75 °C for 3 min and slowly cooled down to 22 °C. The sequences of the oligonucleotides used in this study are shown in Table 1.

Primer Extension Reactions. Primer extension reactions were carried out in 20 μL of reaction buffer containing 30 mM 4-(2-hydroxyethyl)-1-piperazineethanesulfonic acid (HEPES, pH 7.0), 8% glycerol, 0.1 mg/mL bovine serum albumin, 10 mM $MgCl_2$ or 1 mM $MnCl_2$, 20 nM DNA substrate, 200 μM deoxynucleotide triphosphates (dNTPs), and 150 or 400 nM PrimPol. Some reactions were supplemented with 300 nM PolDIP2 or 20 nM RPA and 30 nM four-subunit yeast Pol ζ. Optimal concentrations of RPA and PolDIP2 for primer extension reactions were determined previously.[44] Reaction mixtures were prepared on ice, and DNA polymerization was initiated by adding dNTPs. Tubes were immediately placed in a water bath preheated at 37 °C and were incubated for 10 min or as indicated in figure legends. The reactions were terminated by adding 20 μL of loading buffer containing 95% formamide, 10 mM ethylenediaminetetraacetic acid (EDTA), and 0.1% bromophenol blue. DNA products were resolved on 21% polyacrylamide gels containing 7 M urea followed by phosphorimaging on Typhoon 9400 (GE Healthcare). Experiments were repeated three times. The percentage of extension was calculated by dividing the amount of extended primer by the amount of all labeled DNA bands for each reaction, and it is shown in the diagrams as "PrExt" (primer extension). The percentage of bypassed lesion ("LsBp" in Figure 2) was calculated by dividing the amount of DNA products with nucleotide incorporated opposite the lesion and lesion bypassed DNA products by the amount of all labeled DNA bands in a lane. The mean values of primer extension and bypassed lesion with the standard errors were calculated.

Steady-State Kinetics Analysis of dNMP Incorporation. To quantify the incorporation of individual dNMPs in opposite DNA lesions, we varied each dNMP concentration from 0.03 to 3000 μM in the reactions. 20 nM DNA substrate and 100 nM PrimPol were used in all experiments. Despite the excess of PrimPol over DNA, reactions reached a steady-state (rate-limiting step). 300 nM PolDIP2 and 20 nM RPA were added in reactions in several experiments. The reactions were incubated for different time intervals (from 30 s to 10 min) to ensure that about 20−40% of the primer is

Table 1. Oligonucleotides Used in the Study

15-mer primer	5′-CGTACTCGTAGGCAT-3′
11-mer primer	5′-CGTACTCGTAG-3′
50-mer template	5′-TCCTACCGTGCCTACCTGAACAGCTGGTCACACTXATGCCTACGAGTACG-3′ X = dG or N^2-dG adduct

https://doi.org/10.1021/acschembio.2c00717
ACS Chem. Biol. 2022, 17, 3238−3250

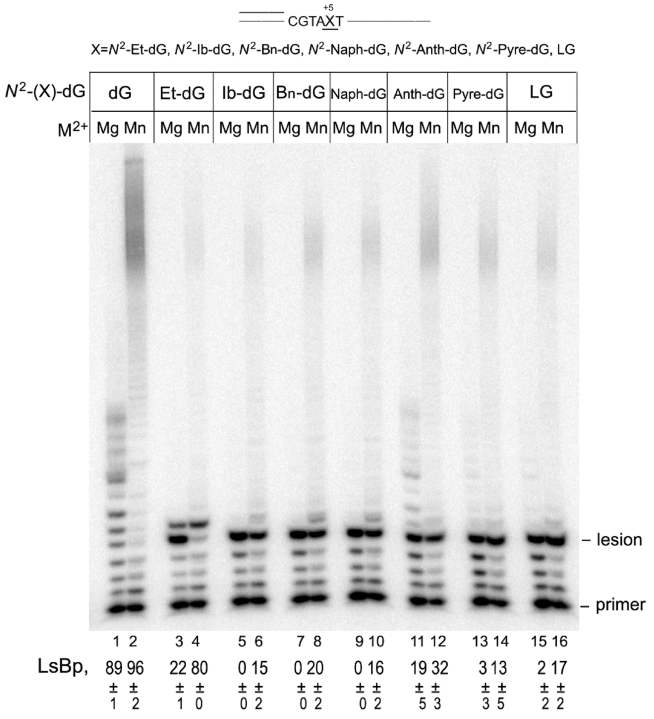

Figure 2. TLS activity of PrimPol opposite N^2-dG adducts. Running start primer extension reactions in the presence of 400 nM PrimPol, Mg^{2+}, or Mn^{2+} ions and an equimolar dNTP mixture. N^2-dG lesions are located in the +5-template position upstream of the primer.

utilized at the maximum dNTP concentration. Calculations were made using GraFit software (Erithacus Software, UK). The data were fit to the Michaelis–Menten equation $V = V_{MAX} \times [dNTP])/(K_M + [dNTP])$, where V and V_{MAX} are the observed and the maximum rates of the reaction (in percentages of utilized primer per minute), respectively, and K_M is the apparent Michaelis constant. The calculated apparent K_M and V_{MAX} parameters were used to determine the catalytic efficiency (V_{MAX}/K_M) and the fidelity of dNTP incorporation (V_{MAX}/K_M for incorrect dNTP divided by V_{MAX}/K_M for the correct substrate). Experiments were repeated three times, and data are reported with the estimated standard error.

Molecular Dynamics Simulations. The recently reported crystal structure of PrimPol (PDB ID: 7JK1)[48] was used for the modeling studies. The 8-oxo-G lesion was replaced by N^2-Et-dG, N^2-Ib-dG, and N^2-Bn-dG adducts and an unmodified complex was also generated as the reference structure. The force field for the ethyl and isobutyl was prepared in the R.E.D server using the reported protocols, at a theory level of HF/6-31G* in Gaussian 16, revision B.01 version (Supplementary Figures S1 and S2).[49−51] For dCTP and N^2-Bn-dG adduct, the previously reported force fields were used (https://upjv.q4md-forcefieldtools.org/REDDB/projects/F-90/).[47] The DNA sequences were not altered during the study. The missing residues in the protein were filled in using the loop modeler script of MODELLER software.[52] The 8-oxo-G was converted to dG in the tleap (AMBER 18)[53] to prepare the unmodified structure. The Ca^{2+} in the structure was replaced by a Mg^{2+} ion and an additional Mg^{2+} ion was added at the active site of the polymerase. The simulations were also carried out using the same protocol using Mn^{2+} ions in the place of Mg^{2+}.

The ff14SB force field[54] was used for the protein, bsc1 force field[55] for the DNA, and the TIP3P water model for water and counter ions. Na^+ ions were added to neutralize the system and were immersed in a water box of 10.0 Å. Complexes were minimized in two stages: 10,000 steps of steepest descent minimization with restraints on the protein, nucleic acid, and Mg^{2+} and another 10,000 steps without any restraints. The systems were then heated to 300 K in 200 ps with slight restraints of 10 kcal/mol $Å^2$ on protein, nucleic acid, and Mg^{2+} ions in the *NVT* ensemble. Then 5 ns *NPT* equilibration and 200 ns *NPT* production simulation were done using the graphics processing unit accelerated version of PMEMD[56,57] in AMBER 18. The SHAKE algorithm was applied to bonds containing hydrogen. The analysis was done using CPPTRAJ AmberTools 19 and visual molecular dynamics (MD).[58] Pictures were rendered using PyMOL (Schrodinger LLC). The running averages are represented in all the distance and RMSD plots.

RESULTS

PrimPol Incorporates dCMP Opposite N^2-Ethyl-dG but Is Blocked by Bulky N^2-dG Adducts in Mg^{2+} Reactions. In this work, several N^2-adducts of guanine were studied with PrimPol: N^2-Et-dG, N^2-Ib-dG, N^2-Bn-dG, N^2-Naph-dG, N^2-Anth-dG, N^2-Pyre-dG, and LG (Figure 1). The formation and synthesis of these DNA adducts have been discussed previously.[23,47]

To evaluate the ability of human PrimPol to synthesize past N^2-dG adducts, primer extension reactions in the presence of Mg^{2+} (10 mM) or Mn^{2+} (1 mM) ions and 400 nM PrimPol were carried out. In the running start assay, PrimPol incorporated dNMPs opposite N^2-ethyl-dG (+5 position upstream of the primer) but could not extend DNA synthesis beyond the lesion in Mg^{2+}-reactions (Figure 2, lane 3). In the presence of Mn^{2+} ions, incorporating dNMPs opposite N^2-Et-dG was more efficient, and a weak extension was observed (Figure 2, lane 4). In the running start reactions, bulky N^2-dG adducts blocked the TLS activity of PrimPol when Mg^{2+} was used (Figure 2, lanes 5, 7, 9, 11, 13, and 15). At the same time, PrimPol could replicate past all of the N^2-dG adducts with low efficiency in the presence of Mn^{2+} ions (Figure 2, lanes 6, 8, 10, 12, 14, and 16). Unexpectedly, lesion bypass with very low efficiency was also observed on the DNA template with N^2-Anth-dG in Mg^{2+}-reactions (Figure 2, lane 11). Trace lesion bypass activity was also detected on DNA with N^2-Pyre-dG and LG adducts in the presence of Mg^{2+} ions (Figure 2, lanes 13 and 15).

We also analyzed the single nucleotide incorporation opposite N^2-dG adducts in primer extension standing start reactions and steady-state kinetics experiments. PrimPol incorporated only complementary dCMP on DNA containing relatively nonbulky N^2-Et-dG when Mg^{2+} ions were used in reactions (Figure 3, lane 15). The incorporation of dCMP opposite N^2-Et-dG was about 87-fold less efficient than opposite undamaged dG (Table 2). In contrast, Mn^{2+} ions stimulated the incorporation of all dNMPs on DNA templates with all tested N^2-dG adducts (Figure 3, lanes 17−20, 27−30, 37−40, 47−50, 57−60, 67−70, 77−80).

In reactions with bulky N^2-Naph-dG, N^2-Pyre-dG, and LG lesions, PrimPol preferably incorporated noncomplementary dAMP and less efficiently dGMP. The template DNA contains T and C in the +2 and +3 positions, and PrimPol likely incorporates complementary purine dNMPs opposite pyrimidines using the lesion "skipping" mechanism. It is possible that weak TLS activity on DNA with bulky N^2-Anth-dG, N^2-Pyre-dG, and LG lesions in Mg^{2+}-reactions (Figure 2, lanes 11, 13, 15 and Figure 3, lanes 51, 61, 71) is also generated by the lesion "skipping" mechanism.

RPA and PolDIP2 Stimulate the TLS Activity of PrimPol on DNA with N^2-dG Adducts. RPA regulates PrimPol access to DNA in response to replication stress in vivo[7,8,59] and stimulates the DNA polymerase and DNA primase activities of PrimPol in vitro.[7,60] PolDIP2 was also

https://doi.org/10.1021/acschembio.2c00717
ACS Chem. Biol. 2022, 17, 3238−3250

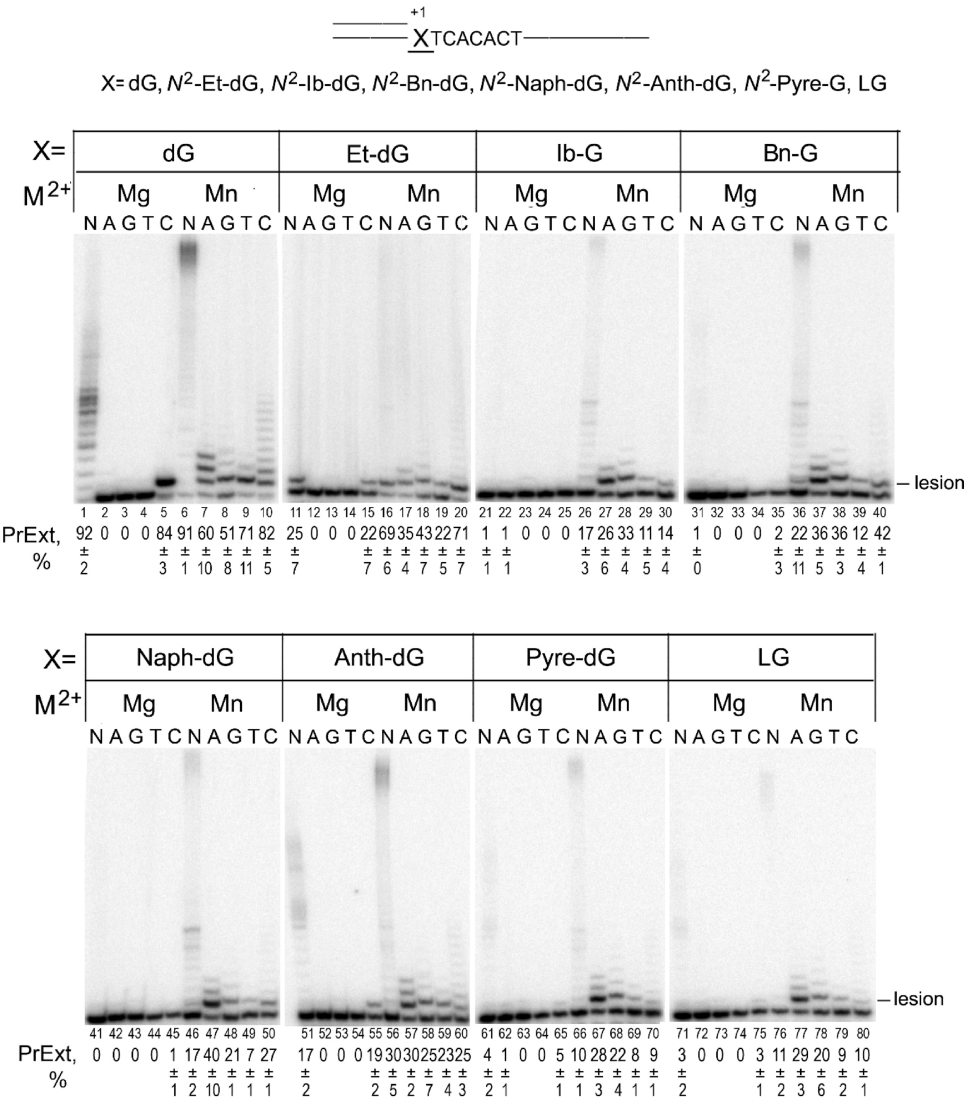

Figure 3. Individual dNMP incorporation opposite dG and N^2-dG adducts. Standing start primer extension reactions in the presence of 400 nM PrimPol and Mg^{2+} (10 mM) or Mn^{2+} (1 mM) ions. Reactions were incubated for 10 min. N^2-dG lesions are located in the +1-template position upstream of the primer. N − an equimolar dNTP mixture, A − deoxyadenosine triphosphate (dATP), G − deoxyguanosine triphosphate (dGTP), T − deoxythymidine triphosphate (dTTP), and C − dCTP.

Table 2. Steady-State Kinetic Parameters for dCMP Incorporation Opposite dG and N^2-Et-dG by PrimPol (Mg^{2+} Ions)

template	K_M, μM	V_{MAX}, %/min	V_{MAX}/K_M	F_{inc}
dG	273 ± 64	83.3 ± 3.2	0.323 ± 0.06	1
N^2-Et-dG	2283 ± 184	8.1 ± 0.7	0.0037 ± 0.00009	87-fold

shown to stimulate the TLS activity of PrimPol.[41,61] To analyze the effect of RPA and PolDIP2 on N^2-dG adduct bypass by PrimPol, we carried out primer extension reactions with 150 nM of PrimPol and 300 nM of PolDIP2 (2-fold excess of PolDIP2) or 20 nM of RPA (1:1 RPA/DNA ratio) (Figure 4). RPA and PolDIP2 stimulated the DNA polymerase activity of PrimPol on undamaged dG in the presence of Mg^{2+} and promoted the extension reaction (Figure 4A, lanes 6−15). Both accessory proteins also increased the efficiency of dNMP incorporation opposite N^2-Et-dG (Figure 4). Nevertheless, RPA and PolDIP2 did not improve the TLS activity of PrimPol on bulky N^2-dG adducts in Mg^{2+} reactions (data are not shown).

In the presence of Mg^{2+} ions, RPA and PolDIP2 slightly increased the incorporation of noncomplementary dAMP, dGMP, and dTMP opposite dG (Figure 5A, lanes 7−8 and 12−14) and dGMP opposite N^2-Et-dG (Figure 5A, 23 and 28). PolDIP2 also visibly changed the spectrum of dNMP incorporation on DNA templates with dG and N^2-Et-dG in the presence of Mn^{2+} ions (Figure 5B,D), increasing the incorporation of dAMP, dGMP, and dTMP on the undamaged template and template with N^2-Et-dG (Figure 5B, lanes 7−9, 22−24).

However, kinetics analysis of dNMP incorporation showed that PolDIP2 increased the incorporation efficiency of all nucleotide substrates (Table 3). The incorporation of noncomplementary nucleotide substrates can be mediated by the lesion "skipping" mechanism: dAMP opposite +2T, dGMP opposite +3C, and dTMP opposite +4A. Together, these data suggest that accessory factors, RPA and PolDIP2,

https://doi.org/10.1021/acschembio.2c00717
ACS Chem. Biol. 2022, 17, 3238−3250

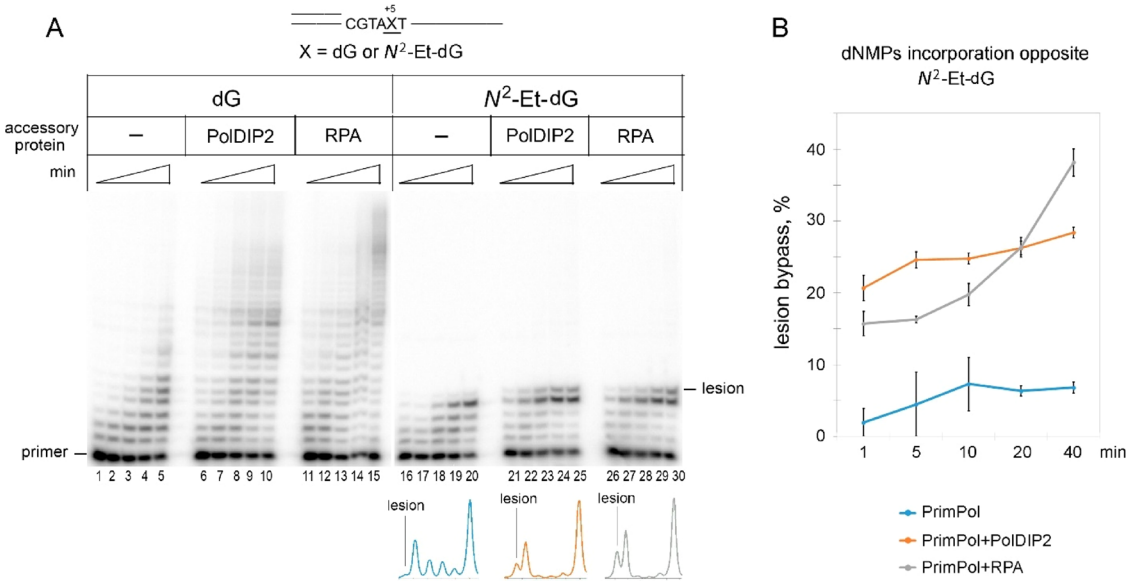

Figure 4. TLS activity of PrimPol opposite N^2-dG adducts in the presence of PolDIP2 and RPA. (A). Running start primer extension reactions with Mg^{2+} ions, and an equimolar dNTP mixture in the absence or the presence of PolDIP2 or RPA. The spectrum of dNMP incorporation on the DNA template with N^2-Et-dG lesion located in the +5-template position is shown (for lanes with 40−50% primer utilization). (B). Diagram showing the percent of dNMP incorporation opposite N^2-Et-dG in the absence or the presence of PolDIP2 or RPA. Concentration of PrimPol was reduced to 150 nM to keep the PrimPol:PolDIP2 ratio = 1:2. Note that the inhibition of activity by salt from the PolDIP2/RPA storage buffer is observed both in experimental and control reactions.

stimulate nucleotide incorporation by PrimPol on undamaged DNA and DNA template with nonbulky N^2-Et-dG lesion.

Pol ζ_4 Extends the dC-N^2-Et-dG Pair Synthesized by PrimPol. Eukaryotic Pol ζ efficiently extends mismatched primer termini and primer termini paired with DNA lesions and cooperates with DNA polymerases to bypass various DNA lesions.[62] Yeast Pol ζ_4 efficiently extends PrimPol-generated primer termini paired with the 1,2-d(GpG) intrastrand cross-link in vitro.[41] We analyzed the combined TLS activity of PrimPol and Pol ζ_4. Only a small amount of the full-length DNA products was observed in reactions with Pol ζ_4 alone on DNA containing N^2-Et-dG lesion (Supplementary Figure S3). In contrast, efficient N^2-Et-dG bypass was observed when Pol ζ_4 was added to reactions in combination with PrimPol, suggesting that Pol ζ_4 is an efficient extender of the dC-N^2-Et-dG pair synthesized by PrimPol.

Structural Parameters Required for Successful Replication by PrimPol. To rationalize the experimental observation on TLS across N^2-Et-dG, N^2-Ib-dG, and N^2-Bn-dG adducts having different steric bulkiness, molecular modeling and MD simulations (200 ns) were carried out for the insertion stage of the DNA-PrimPol-incoming nucleotide ternary complexes using AMBER 18. Root mean square deviation (RMSD) of the protein backbone was calculated for all the complexes. The RMSD values indicate that the complexes are well equilibrated and stable during the simulation (Supplementary Figure S4). MD trajectories were used to calculate various structural parameters associated with the insertion stage of replication. For successful replication, specific structural requirements are to be satisfied.[63] These parameters are the optimal reaction distance (3.5 Å) between O3′−Pα of the primer and incoming nucleotide, the attack angle, O3′−Pα−O$\alpha\beta$, of the primer and the incoming nucleotide (150°−180°), and the C1′−C1′ distance (10.8 Å) between the template and incoming nucleotides (Figure 6A). Along with these, a strong Watson crick base-pairing interaction between the incoming nucleotide and the template dG facilitates proper replication.

The reaction distance was constant throughout the simulation in the dG and N^2-Et-dG complexes, but the values are high in the N^2-Ib-dG and N^2-Bn-dG complexes (Figure 6B). Similar to the reaction distance, the attack angle did not satisfy the criteria in the N^2-Ib-dG and the N^2-Bn-dG complexes, but it was within the range for the N^2-Et-dG complex (Figure 6C). The C1′−C1′ distance was high for the N^2-Ib-dG and N^2-Bn-dG complexes but had a value ∼10.8 Å for the N^2-Et-dG complex (Figure 6D). The changes in the reaction parameters correspond to the reorientation of the incoming nucleotide. In the N^2-Bn-dG complex, dCTP gradually moved away from the primer and damaged nucleotide, which is constant in the unmodified complex (Supplementary Figure S5).

Since Mn^{2+} ion is the preferred metal cofactor for the PrimPol, we performed a 200 ns MD simulation in all the four complexes with Mn^{2+} in place of Mg^{2+}. All the parameters corresponding to successful replication were found to have the optimum values in the case of the unmodified and N^2-Et-dG complexes, as those in the presence of Mg^{2+} ions. The N^2-Ib-dG and the N^2-Bn-dG complexes did not satisfy the conditions for successful replication even in the presence of Mn^{2+} ions (Figure S6). To identify any significant difference in the hydration around the Mn^{2+} and Mg^{2+} ions owing to their sizes, the number of water molecules around 5 Å cut off in the vicinity of the metal cofactors was calculated for unmodified and N^2-Et-dG complexes. At a given time, Mn^{2+} is better hydrated with more water molecules around it (Supplementary Figure S7). This means that Mn^{2+} introduces more order in the neighboring water molecules. The conserved water molecules, which are ordered, would enhance the catalytic/enzymatic activity.[64,65] This could be one of the factors contributing to the efficiency of dCTP incorporation across the N^2-Et-dG in the presence of Mn^{2+} ions.

https://doi.org/10.1021/acschembio.2c00717
ACS Chem. Biol. 2022, 17, 3238−3250

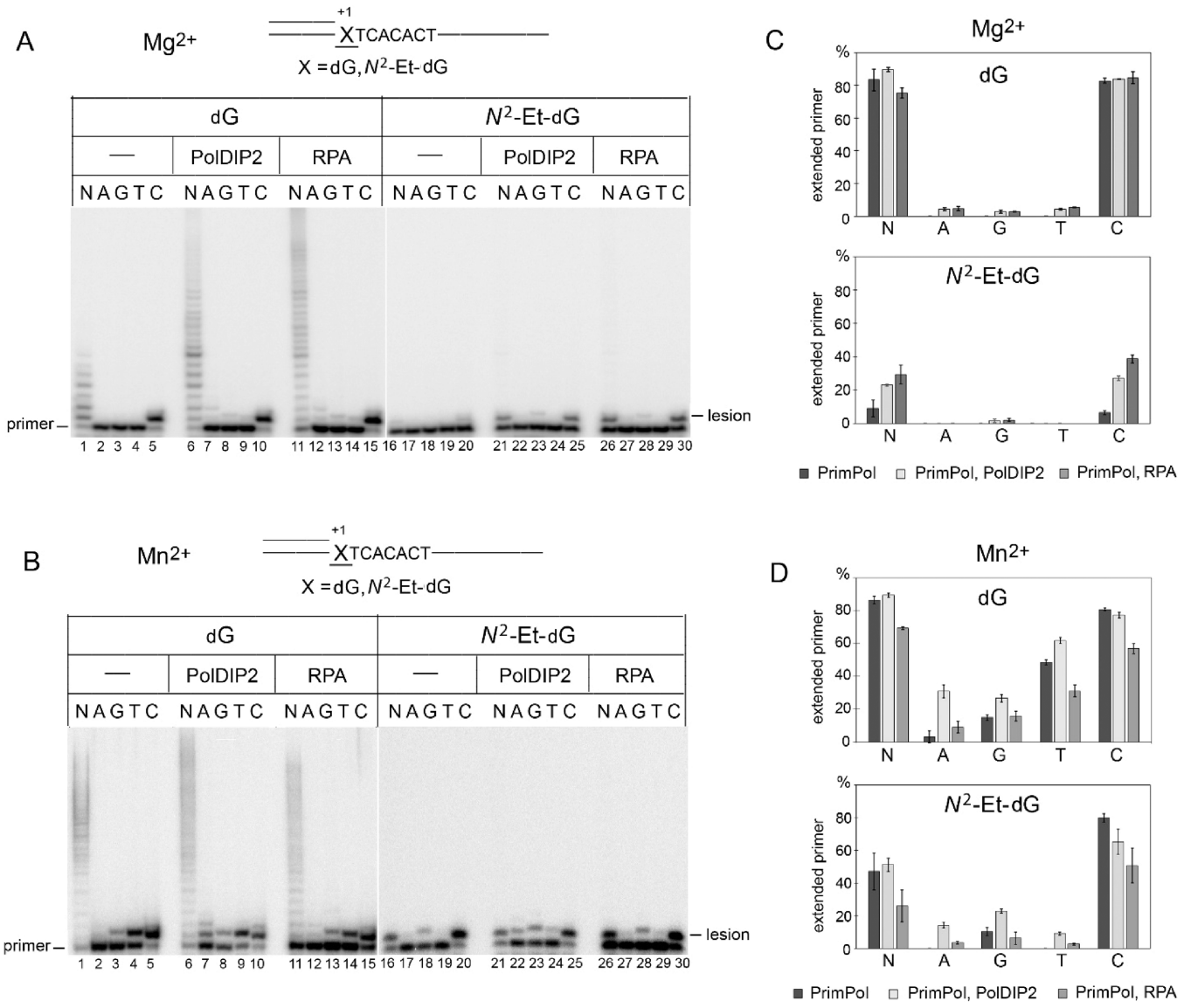

Figure 5. Individual dNMP incorporation opposite dG and N^2-dG adducts in the presence of PolDIP2 and RPA. Standing start primer extension reactions with Mg^{2+} (A) or Mn^{2+} (B) ions. N^2-Et-dG lesion is located in the +1-template position upstream of the primer. Diagrams showing the percent of dNMP incorporation opposite N^2-Et-dG in the presence of PolDIP2 or RPA and Mg^{2+} (C) or Mn^{2+} (D) ions. N − an equimolar dNTP mixture, A − dATP, G − dGTP, T − dTTP, and C − dCTP. Concentration of PrimPol was reduced to 150 nM to keep the PrimPol:PolDIP2 ratio = 1:2. Note that the inhibition of activity by salt from the PolDIP2/RPA storage buffer is observed both in experimental and control reactions. Reactions were incubated for 10 min.

Table 3. Kinetic Parameters for dNMP Incorporation Opposite dG by PrimPol in the Presence of PolDIP2 (Mn^{2+} Ions)

dNMP	proteins	K_M, μM	V_{MAX}, %/min	V_{MAX}/K_M	F_{inc}
dATP	PrimPol	5.7 ± 0.2	1.5 ± 0.02	0.26 ± 0.01	1.4×10^{-2}
	PrimPol + PolDIP2	5.5 ± 0.3	3.6 ± 0.1	0.64 ± 0.02	1.2×10^{-2}
dGTP	PrimPol	7.7 ± 0.1	0.6 ± 0.1	0.08 ± 0.02	4.2×10^{-2}
	PrimPol + PolDIP2	7.6 ± 0.5	1.6 ± 0.4	0.21 ± 0.05	4.0×10^{-3}
dTTP	PrimPol	27.4 ± 3.5	3.8 ± 0.2	0.14 ± 0.01	7.3×10^{-3}
	PrimPol + PolDIP2	25.4 ± 3.8	8.2 ± 0.4	0.33 ± 0.03	6.3×10^{-3}
dCTP	PrimPol	7.6 ± 1.3	140 ± 2	19.2 ± 3.8	1
	PrimPol + PolDIP2	2.2 ± 0.2	110 ± 20	52.2 ± 13	1

The hydrogen bond occupancies between the bases were calculated to determine the interaction between the dCTP and the damaged base (dG*) (Supplementary Table S1). The H-bond occupancies for the N^2-Ib-dG and N^2-Bn-dG complexes were low, indicating the absence of a stable interaction between the dG* and the incoming dCTP. In the N^2-Et-dG complex, strong and stable interactions are maintained between the dG* and dCTP throughout simulations. Altogether, structural parameters show that successful replication conditions are satisfied in the N^2-Et-

https://doi.org/10.1021/acschembio.2c00717
ACS Chem. Biol. 2022, 17, 3238−3250

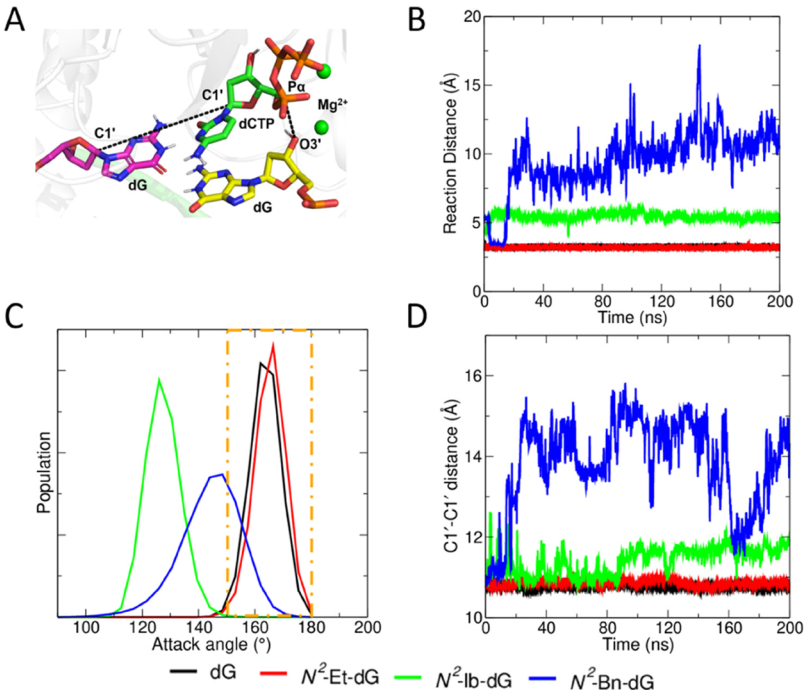

Figure 6. Structural parameters associated with the insertion stage of PrimPol. (A) Representative images of residues and atoms involved in the parameter calculations. (B) Reaction distance calculated between the O3′ of the primer strand and the Pα of dCTP; (C) Attack angle calculated between the O3′ of the primer strand and the Pα, O$\alpha\beta$ of dCTP; D. C1′−C1′ distance between the adduct and dCTP for the various complexes.

dG complex but not in the N^2-Ib-dG and the N^2-Bn-dG complexes.

Interactions of the Active-Site Amino Acid Residues with N^2-Ethyl-dG and the Incoming Nucleotide. The conservative Arg47, Arg288, and Asn289 active-site residues interacting with an incoming nucleotide and Arg76 interacting with the templating base might play a role in the N^2-dG lesion bypass[48,66] (Supplementary Table S2). We analyzed the role of the active-site amino acid residues Arg47, Arg76, Arg288, and Asn289[48,66] in the TLS activity of PrimPol on DNA with N^2-Et-dG (Figure 7). Experiments were carried out in the presence of Mn^{2+} ions since the activity of mutant variants was abolished or severely reduced in Mg^{2+}-reactions. The R47A and R76A substitutions reduced the DNA polymerase activity of PrimPol both on undamaged and damaged DNA. The N289A mutation slightly decreased nucleotide incorporation on undamaged dG (Figure 7A) but improved the TLS activity on the DNA template with N^2-Et-dG (Figure 7B). In contrast, the R288A mutation abolished nucleotide incorporation only opposite N^2-Et-dG (Figure 7B, lanes 22−28). To reach equal levels of DNA polymerase activity on undamaged DNA, we also increased the concentration of mutant variants and incubation time. Under these conditions, the wild-type PrimPol, R47A, and R76A mutant variants incorporated nucleotides opposite N^2-Et-dG with similar efficiency, but the PrimPol variant with the R288A substitution was entirely blocked by the N^2-Et-dG lesion (Supplementary Figure S8).

To understand the role of the Arg288 residue in the TLS across N^2-Et-dG, we analyzed the modeled PrimPol structure with N^2-dG adducts in the dCTP insertion stage. The total number of H-bond contacts made by the dCTP with amino acids of the human PrimPol within 5 Å range were calculated, and specific noncovalent interactions in the active site were investigated by visual inspection of trajectories. As expected, the number of H-bonds decreases with an increase in the bulkiness of the system (Supplementary Figure S9). Arg76 and Asn289 cause steric hindrance to bulky N^2-dG groups. The Arg288 residue stabilizes hydrogen bonding and salt bridge interactions with the incoming nucleotide and the 3′-nucleotide of the primer opposite dG and N^2-Et-dG (Figure 8A,B). These contacts were lost in the N^2-Ib-dG and the N^2-Bn-dG complexes (Figure 8C,D). The H-bond distances between dCTP and Arg288 showed a favorable value in the N^2-Et-dG complex similar to that for the unmodified one (Figure 8E). One specific interaction is the H-bond between the HH11 of R288 and the 4O′ of the dCTP, which is very strong in the dG and N^2-Et-dG adduct. In the case of N^2-Bn-dG, loss of contact was also observed for the Arg76, which makes multiple robust contacts with the unmodified template. Overall, many critical amino acid contacts are lost in the bulkier N^2-dG complexes in the active site of human PrimPol.

DISCUSSION

PrimPol possesses TLS activity and bypasses many nonbulky DNA lesions.[1−3,10−12,67] In this study, we analyzed the TLS activity of PrimPol on DNA templates with bulky N^2-dG adducts and demonstrated that PrimPol incorporates nucleotides only on DNA templates with relatively small N^2-Et-dG lesions and is entirely blocked by large N^2-Ib-dG, N^2-Bn-dG, N^2-Naph-dG, N^2-Anth-dG, N^2-Pyre-dG, and LG adducts in the presence of Mg^{2+} ions. In contrast, PrimPol partially tolerated bulky N^2-dG adducts in the presence of Mn^{2+} ions, possibly by using the lesion "skipping" mechanism.

Limited TLS on the DNA Template with N^2-Et-dG Lesion. No specific repair pathway for the N^2-Et-dG adduct exists,[68,69] and DNA damage tolerance mechanisms play a crucial role in rescuing replication on this lesion. N^2-Et-dG represents a strong block to Pol α[21] but not to Pol δ[22] or TLS polymerases Pol η,[21,22] Pol ι,[24,70] Pol κ,[71] or REV1.[27] Pol η,[21,22,25] Pol κ,[71] and REV1[27] preferentially incorporate

https://doi.org/10.1021/acschembio.2c00717
ACS Chem. Biol. 2022, 17, 3238−3250

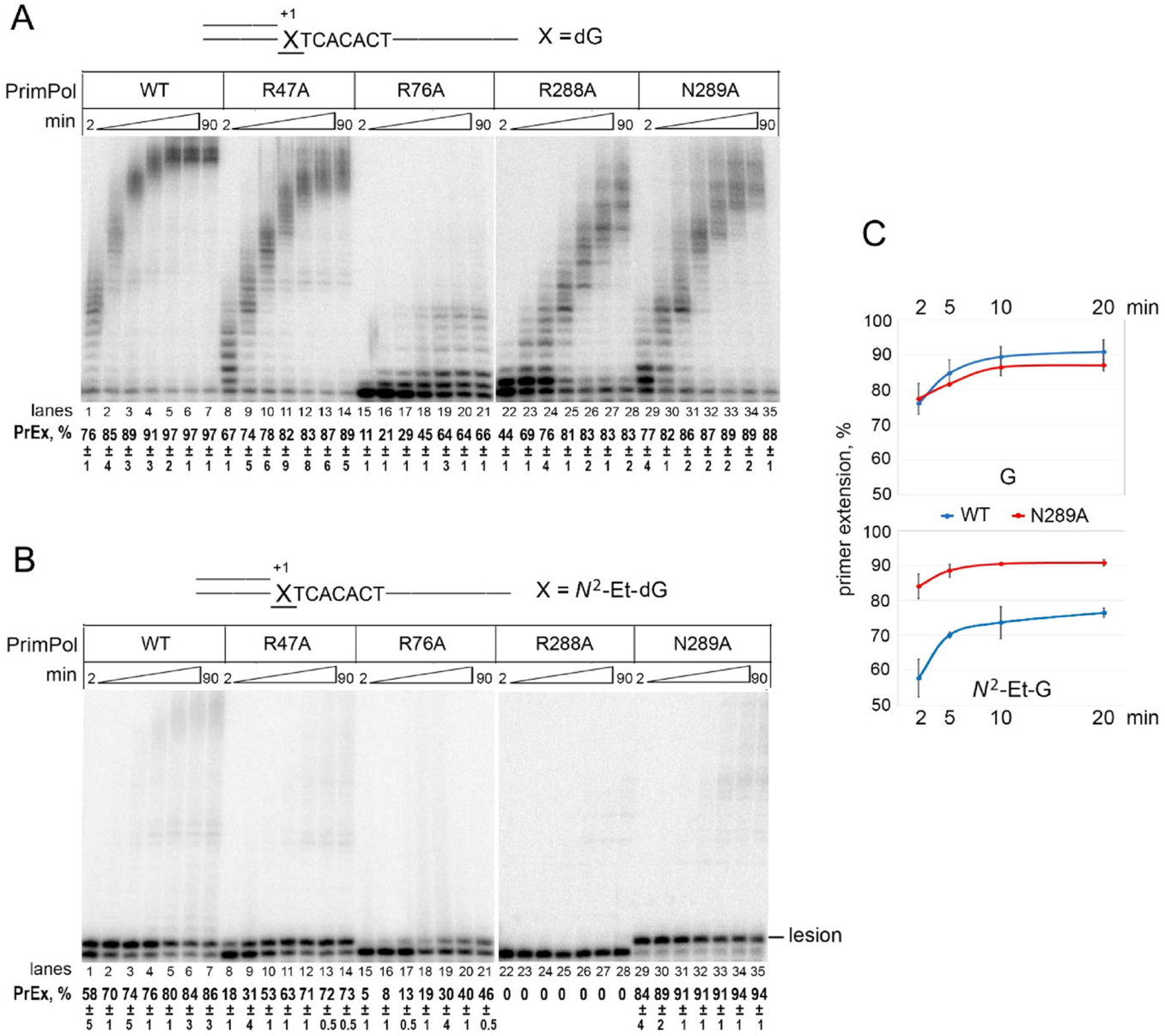

Figure 7. TLS activity of PrimPol variants with R47A, R76A, R288A, and N289A substitutions on DNA substrates with dG and N^2-Et-dG. Standing start primer extension reactions with 150 nM PrimPol, Mn^{2+} ions, and an equimolar dNTP mixture for 2−90 min on undamaged DNA (A) and N^2-Et-dG (B). C. Diagram shows the percent of dNMP incorporation (PrExt, %) opposite N^2-Et-dG by the wild-type and N289A PrimPol variants (2−20 min).

complementary dCMP opposite N^2-Et-dG lesion, however, a high nucleotide misincorporation is observed for Pol α and Pol ι.[21,24]

The efficiency and accuracy of PrimPol on the DNA template with N^2-Et-dG are dependent on divalent metal ions and are modulated by replication accessory factors, PolDIP2 and RPA. In the presence of Mg^{2+} ions, PrimPol incorporated complementary dCMP opposite the N^2-Et-dG adduct with low efficiency. Mn^{2+} ions stimulated the incorporation of the nucleotide opposite N^2-Et-dG but did not improve replication beyond the lesion and increased the incorporation of dGMP and dAMP. These data are in agreement with previous studies. In particular, Mn^{2+} ions stimulate the TLS activity of PrimPol on DNA templates by blocking DNA lesions such as TG, AP-site, εA, photoproducts, and 1,2-intrastrand cisplatin cross-link but decrease the accuracy of nucleotide incorporation.[1,2,10−12,41,67,72] Interestingly, all structural parameters for favorable replication revealed by MD studies were similar in Mg^{2+} and Mn^{2+} complexes except for the number and order of water molecules around the ions. More ordered water molecules around the Mn^{2+} ions might favor the efficient catalytic activity of PrimPol in reactions with Mn^{2+}.[64,65]

It was shown that Mn^{2+} promotes the "skipping" or "template scrunching" mechanism of TLS by PrimPol.[12] This mechanism is likely mediated by flanking microhomologies and is sequence-dependent: PrimPol reanneals the primer to nucleotides downstream of the lesion and loops out the templating lesion.[1,12] Efficient incorporation of dAMP and dGMP observed opposite N^2-Et-dG in Mn^{2+} reactions agrees with the DNA lesion "skipping" mechanism. Mn^{2+} ions likely stimulate nucleotide incorporation opposite +2 and +3 downstream templating nucleotides in the sequence context

https://doi.org/10.1021/acschembio.2c00717
ACS Chem. Biol. 2022, 17, 3238−3250

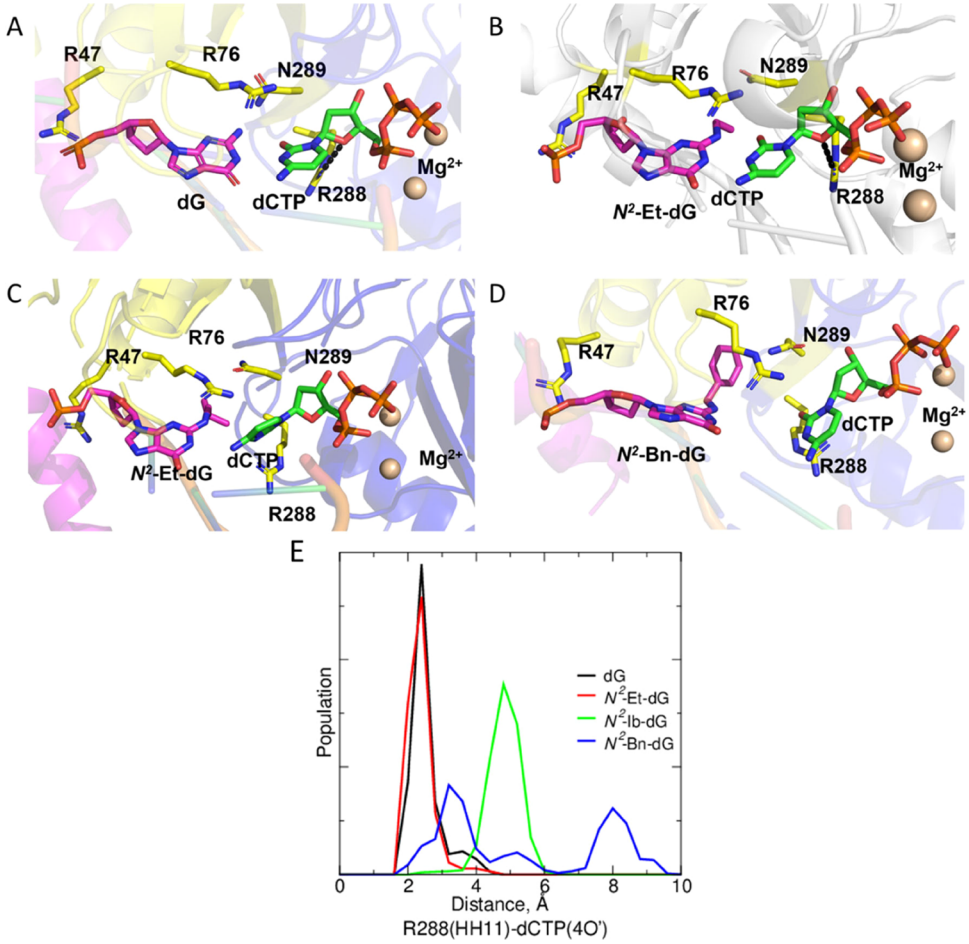

Figure 8. Representative structures showing the orientation of (A) dG; (B) N^2-Et-dG; (C) N^2-Ib-dG; and(D) N^2-Bn-dG in the active site of PrimPol. Initial frame from the 200 ns trajectory is represented here. (E) Population distribution of the H-bond distance between the dCTP and R288 in various N^2-dG lesions. Black dashed line in (A and B) shows the strongest H-bond between R288 and dCTP.

"$(G^X)T_{+2}C_{+3}A$." PrimPol most likely uses the lesion "skipping" mechanism to bypass bulky adducts in the presence of Mg^{2+}. The possible mechanisms for the weak bypass of the N^2-Anth-dG adduct could be attributed to misalignment or template slippage. However, the MD studies with N^2-Anth-dG complexes could not capture this bypass activity (data not shown).

Replication accessory factors, RPA and PolDIP2, interact with PrimPol and might regulate PrimPol TLS activity. RPA directs the localization of PrimPol in DNA in response to DNA damage and replication stress in vivo.[7,8,59] The DNA polymerase,[60,61] strand-displacement,[44] and primase activities of PrimPol[60] are stimulated by PolDIP2 and RPA. Moreover, PolDIP2 enhanced the TLS activity of PrimPol opposite 8-oxo-G and the 1,2-intrastrand cisplatin cross-link.[41,61] The stimulation of the TLS activity of PrimPol by RPA is yet to be demonstrated.

In this work, PolDIP2 and RPA proteins enhanced the TLS activity of PrimPol opposite the N^2-Et-dG adduct without significant change in fidelity. PrimPol alone and in the presence of RPA and PolDIP2 preferentially incorporate complementary dCMP opposite the lesion in reactions with Mg^{2+} and Mn^{2+} ions. However, PrimPol could not extend beyond the N^2-Et-dG even in the presence of accessory proteins. To bypass the lesion in vivo, PrimPol would require an extender polymerase. Pol ζ readily extends from N^2-dG adducts bypassed by REV1.[73] We also showed that Pol ζ_4 efficiently extends from primer termini paired with N^2-Et-dG by PrimPol in vitro. However, PrimPol and Pol ζ_4 work in different pathways, and cooperation in vitro may not be relevant in vivo.

Bulky N^2-dG Adducts Block PrimPol. Depending on the size and shape of the aromatic ring system, N^2-dG adducts impart steric hindrance to DNA-polymerases activity.[74] Many bulky N^2-dG adducts represent a strong block to replication for high-fidelity DNA polymerases and TLS polymerases.[18,22,24,26] Eukaryotic Y-family DNA polymerases have different abilities to bypass bulky N^2-dG adducts. Pol ι demonstrates relatively effective and error-prone bypass of N^2-Me-dG, N^2-Et-dG, N^2-Ib-dG, and N^2-Bn-dG, but adducts of N^2-Naph-dG size and larger almost completely inhibit Pol ι activity.[24,26] Human Pol η is slightly more effective in replicating bulky N^2-dG adducts and bypasses lesions from N^2-Me-dG to N^2-Naph-dG in a relatively error-free manner.[22] Yet adducts of N^2-Anth-dG size and bulkier significantly decrease the TLS activity of Pol η and enhance nucleotide misincorporation.[22,26,75] Pol κ and REV1 replicate past a wide range of bulky N^2-dG adducts with efficiency and fidelity equal to replication on undamaged dG.[25,27,73]

Unlike Y-family DNA polymerases, human PrimPol was incapable of nucleotide incorporation opposite the majority of bulky N^2-dG adducts in the presence of Mg^{2+} ions starting

https://doi.org/10.1021/acschembio.2c00717
ACS Chem. Biol. 2022, 17, 3238−3250

from N^2-Ib-dG. However, Mn^{2+} ions stimulated weak lesion bypass on DNA templates with all studied N^2-dG adducts and significantly increased the misincorporation of dAMP and dGMP, possibly utilizing a lesion "skipping" mechanism. Importantly, neither PolDIP2 nor RPA stimulated the TLS activity of PrimPol on bulky N^2-dG adducts in the presence of Mg^{2+} or Mn^{2+} ions.

To date, a few crystal structures are available of PrimPol harboring dT as template nucleotide and incoming dATP[66] and template 8-oxo-dG and incoming dCTP/dATP capturing the insertion stage.[48] The structures show that the PrimPol active-site cleft is relatively constrained. The active site at the minor groove side of DNA contains residues Arg76 and Asn289 located at a short distance from template DNA, leaving no space to accommodate bulky adducts and incorporate nucleotides opposite N^2-dG lesions. The location of these amino acids close to the template can explain the relatively poor ability of PrimPol to bypass even the N^2-Et-dG adduct. Indeed, the N289A mutation slightly increased the efficiency of dCMP incorporation opposite N^2-Et-dG lesion by PrimPol. Nevertheless, the N^2-Et-dG complex retains key contacts behaving similarly to the unmodified complex. The bulky N^2-Ib-dG and N^2-Bn-dG adducts cause reorientation of the position of the catalytic amino acids, which results in the loss of many critical interactions in the active site (Supplementary Figures S9 and S10).

We also demonstrated that the mutation of the conserved Arg288 contacting the incoming dCTP abolishes nucleotide incorporation opposite the N^2-Et-dG lesion and significantly affects the dCTP dynamics. This is also reflected in the H-bond between the damaged dG and dCTP and the structural parameters (C1′−C1′, distance, reaction distance, and attack angle) required for the successful replication. The extent of variations in the satisfactory criteria for replication is directly related to the steric bulkiness of the adduct.

Stimulation of PrimPol Activity by RPA Depends on the DNA Structure and Reaction Conditions. RPA shows a stable 30 nt binding mode[76,77] and efficiently stimulates PrimPol on DNA templates with long single-stranded DNA.[7,60] However, Martínez-Jiménez et al. demonstrated that RPA inhibits PrimPol activity on the 65-mer DNA substrate with 49 nt ssDNA region[60] suggesting that RPA is competing with PrimPol for the primer-template junction in reactions with excess RPA over DNA (12−200 nM RPA/2 nM DNA). In this work, RPA stimulated PrimPol activity even on the 50 nt length DNA substrate containing only the 35−40 nt ssDNA binding site at the equimolar RPA/DNA ratio. Importantly, RPA stimulated the formation of the full-length products by PrimPol on the 50-mer substrate but reduced the amount of primer utilized by PrimPol in Mn^{2+} reactions (lanes 1 and 11, Figure 5B,D). However, in similar reaction conditions, we observed the strong inhibition of PrimPol by RPA on a short 30-mer DNA substrate with a 15−17 nt ssDNA region (data not shown). These data are in agreement with the competition between RPA and PrimPol for the primer-template junction preventing other PrimPol molecules from DNA binding (at least in the presence of Mn^{2+}).

Interestingly, previously we also observed the stimulation of the strand-displacement activity of PrimPol on double-stranded DNA substrate with the 5-nt single-stranded DNA (ssDNA) gap.[44] It was shown that RPA also utilizes an ssDNA binding site size of 4−10 nucleotides and contacts flap in DNA with a short gap.[78,79] We suggest that RPA can increase the processivity of PrimPol using a short ssDNA binding site, and PrimPol can be attracted to the ssDNA-part of the gap from the 5′-side by RPA associated with the flap. Thus, the interaction of PrimPol with RPA may play an important role in the regulation of activity and lesion bypass by PrimPol.

CONCLUSIONS

Human PrimPol possesses TLS activity opposite the N^2-Et-dG adduct by incorporating complementary dCMP. This activity is stimulated by Mn^{2+} ions and accessory proteins, PolDIP2 and RPA. PrimPol activity is blocked by bulky carcinogenic N^2-dG adducts causing the reorientation of the incoming nucleotide and thereby causing the loss of key protein contacts. Our studies show that the steric bulkiness of the adducts can be a limiting factor for efficient DNA synthesis across minor groove adducts by human PrimPol.

ASSOCIATED CONTENT

Supporting Information

The Supporting Information is available free of charge at https://pubs.acs.org/doi/10.1021/acschembio.2c00717.

Cartesian coordinates and restrained electrostatic potential fitting charges of the adducts, TLS activity of PrimPol and Pol ζ_4 with N^2-Et-dG, RMSD of the c-α atoms of the various N^2-dG complexes, representative images showing reorientation of adducts and altering reaction parameters, structural parameters for the successful replication in the simulations with Mn^{2+} ions, total number of water molecules around the metal cofactors, TLS activity of PrimPol mutants on DNA substrates with dG and N^2-Et-dG, population distribution of H-bond count between dCTP and the protein network in N^2-dG complexes, reorientation of catalytic amino acids, adducts and incoming nucleotide in N^2-Ib-dG and N^2-Bn-dG complexes during the simulation, hydrogen bond occupancy between the DNA adduct and dCTP, and role of the conservative active-site residues contacting an incoming nucleotide and the template base (PDF)

AUTHOR INFORMATION

Corresponding Authors

Pushpangadan I. Pradeepkumar − *Department of Chemistry, Indian Institute of Technology Bombay, Mumbai 400076, India;* orcid.org/0000-0001-9104-3708; Email: pradeep@chem.iitb.ac.in

Alena V. Makarova − *Institute of Molecular Genetics, National Research Center Kurchatov Institute, Moscow 123182, Russia;* orcid.org/0000-0002-6513-892X; Email: amakarova-img@yandex.ru

Authors

Elizaveta O. Boldinova − *Institute of Molecular Genetics, National Research Center Kurchatov Institute, Moscow 123182, Russia*

Pratibha P. Ghodke − *Department of Chemistry, Indian Institute of Technology Bombay, Mumbai 400076, India*

Sruthi Sudhakar − *Department of Chemistry, Indian Institute of Technology Bombay, Mumbai 400076, India*

Vipin Kumar Mishra − *Department of Chemistry, Indian Institute of Technology Bombay, Mumbai 400076, India*

https://doi.org/10.1021/acschembio.2c00717
ACS Chem. Biol. 2022, 17, 3238−3250

Anna A. Manukyan − *Institute of Molecular Genetics, National Research Center Kurchatov Institute, Moscow 123182, Russia*
Nataliya Miropolskaya − *Institute of Molecular Genetics, National Research Center Kurchatov Institute, Moscow 123182, Russia*

Complete contact information is available at: https://pubs.acs.org/10.1021/acschembio.2c00717

Author Contributions

[§]E.O.B., P.P.G., and S.S. have contributed equally to this study.

Funding

This work was supported by the DST-RFBR, Indo Russian Joint Grant INT/RUS/RFBR/371 (to PIP) and RFBR-Russia grant 19-54-45035 (to M.N.). The studies of the role of the active-site residues in TLS were supported by RSF grant 18−14-00354 (to M.A.V.). E.O.B. thanks RFBR (PhD fellowship 19-34-90147). S.S. thanks Prime Minister's Research Fellowship (PMRF) for the PhD fellowship, and V.K.M. thanks IIT Bombay for the institute postdoctoral fellowship. We thank Spacetime HPC, IIT Bombay, for the computing facilities.

Notes

The authors declare no competing financial interest.

REFERENCES

(1) García-Gómez, S.; Reyes, A.; Martínez-Jiménez, M. I.; Chocrón, S.; Mourón, S.; Terrados, G.; Powell, C.; Salido, E.; Méndez, J.; Holt, I. J.; Blanco, L. PrimPol, an Archaic Primase/Polymerase Operating in Human Cells. *Mol. Cell* **2013**, *52*, 541−553.
(2) Bianchi, J.; Rudd, S. G.; Jozwiakowski, S. K.; Bailey, L. J.; Soura, V.; Taylor, E.; Stevanovic, I.; Green, A. J.; Stracker, T. H.; Lindsay, H. D.; Doherty, A. J. Primpol bypasses UV photoproducts during eukaryotic chromosomal DNA replication. *Mol. Cell* **2013**, *52*, 566−573.
(3) Mourón, S.; Rodriguez-Acebes, S.; Martínez-Jiménez, M. I.; García-Gómez, S.; Chocrón, S.; Blanco, L.; Méndez, J. Repriming of DNA synthesis at stalled replication forks by human PrimPol. *Nat. Struct. Mol. Biol.* **2013**, *20*, 1383−1389.
(4) Kobayashi, K.; Guilliam, T. A.; Tsuda, M.; Yamamoto, J.; Bailey, L. J.; Iwai, S.; Takeda, S.; Doherty, A. J.; Hirota, K. Repriming by PrimPol is critical for DNA replication restart downstream of lesions and chain-terminating nucleosides. *Cell Cycle* **2016**, *15*, 1997−2008.
(5) Schiavone, D.; Jozwiakowski, S. K.; Romanello, M.; Guilbaud, G.; Guilliam, T. A.; Bailey, L. J.; Sale, J. E.; Doherty, A. J. PrimPol Is Required for Replicative Tolerance of G Quadruplexes in Vertebrate Cells. *Mol. Cell* **2016**, *61*, 161−169.
(6) Torregrosa-Muñumer, R.; Forslund, J.; Goffart, S.; Pfeiffer, A.; Stojkovic, G.; Carvalho, G.; Al-Furoukh, N.; Blanco, L.; Wanrooij, S.; Pohjoismäki, J. L. O. PrimPol is required for replication reinitiation after mtDNA damage. *Proc. Natl. Acad. Sci. U. S. A.* **2017**, *114*, 11398−11403.
(7) Guilliam, T. A.; Brissett, N. C.; Ehlinger, A.; Keen, B. A.; Kolesar, P.; Taylor, E.; Bailey, L. J.; Lindsay, H. D.; Chazin, W. J.; Doherty, A. J. Molecular basis for PrimPol recruitment to replication forks by RPA. *Nat. Commun.* **2017**, *8*, 15222.
(8) Guilliam, T. A.; Jozwiakowski, S. K.; Ehlinger, A.; Barnes, R. P.; Rudd, S. G.; Bailey, L. J.; Skehel, J. M.; Eckert, K. A.; Chazin, W. J.; Doherty, A. J. Human PrimPol is a highly error-prone polymerase regulated by single-stranded DNA binding proteins. *Nucleic Acids Res.* **2015**, *43*, 1056−1068.
(9) Piberger, A. L.; Bowry, A.; Kelly, R.; Walker, A. K.; Gonzalez, D.; Bailey, L. J.; Doherty, A. J.; Mendez, J.; Morris, J. R.; Bryant, H. E.; Petermann, E. PrimPol-dependent single-stranded gap formation mediates homologous recombination at bulky DNA adducts. *Nat. Commun.* **2020**, *11*, 5863.
(10) Stojkovic, G.; Makarova, A. V.; Wanrooij, P. H.; Forslund, J.; Burgers, P. M. J.; Wanrooij, S. Oxidative DNA damage stalls the human mitochondrial replisome. *Sci. Rep.* **2016**, *6*, 28942.
(11) Makarova, A. V.; Boldinova, E. O.; Belousova, E. A.; Lavrik, O. I. In vitro lesion bypass by human PrimPol. *DNA Repair* **2018**, *70*, 18−24.
(12) Martínez-Jiménez, M. I.; García-Gómez, S.; Bebenek, K.; Sastre-Moreno, G.; Calvo, P. A.; Díaz-Talavera, A.; Kunkel, T. A.; Blanco, L. Alternative solutions and new scenarios for translesion DNA synthesis by human PrimPol. *DNA Repair* **2015**, *29*, 127−138.
(13) John, K. Heterocyclic Amines. *Encyclopedia of Cancer*, 2017, vol 3; pp 2066−2072.
(14) Turesky, R. J. Aromatic Amines and Heterocyclic Aromatic Amines: From Tobacco Smoke to Food Mutagens. *Chem. Biol. DNA Damage* **2010**, *2010*, 157−183.
(15) Penning, T. M. Polycyclic Aromatic Hydrocarbons: Multiple Metabolic Pathways and the DNA Lesions Formed. *Chem. Biol. DNA Damage* **2010**, *2010*, 131−155.
(16) Medeiros, M. H. G. DNA damage by endogenous and exogenous aldehydes. *J. Braz. Chem. Soc.* **2019**, *30*, 2000−2009.
(17) Ghodke, P. P.; Harikrishna, S.; Pradeepkumar, P. I. Synthesis and Polymerase-Mediated Bypass Studies of the N 2 - Deoxyguanosine DNA Damage Caused by a Lucidin Analogue. *J. Org. Chem.* **2015**, *80*, 2128−2138.
(18) Ghodke, P. P.; Gore, K. R.; Harikrishna, S.; Kottur, J.; Nair, D. T.; Pradeepkumar, P. I. The N2-Furfuryl-Deoxyguanosine (fdG) Adduct Does Not Alter the Structure of B-DNA. *J. Org. Chem.* **2016**, *81*, 502−511.
(19) Guengerich, F. P. Interactions of Carcinogen-Bound DNA with Individual DNA Polymerases. *Chem. Rev.* **2006**, *106*, 420−452.
(20) Hsu, G. W.; Kiefer, J. R.; Burnouf, D.; Becherel, O. J.; Fuchs, R. P. P.; Beese, L. S. Observing Translesion Synthesis of an Aromatic Amine DNA Adduct by a High-fidelity DNA Polymerase. *J. Biol. Chem.* **2004**, *279*, 50280−50285.
(21) Perrino, F. W.; Blans, P.; Harvey, S.; Gelhaus, S. L.; Mcgrath, C.; Akman, S. A.; Jenkins, G. S.; Lacourse, W. R.; Fishbein, J. C. The N2-Ethylguanine and the O6-Ethyl- and O6-Methylguanine Lesions in DNA: Contrasting Responses from the "Bypass" DNA Polymerase η and the Replicative DNA Polymerase a. *Chem. Res. Toxicol.* **2003**, *16*, 1616−1623.
(22) Choi, J.; Guengerich, F. P. Adduct Size Limits Efficient and Error-free Bypass Across Bulky N 2 -Guanine DNA Lesions by Human DNA Polymerase h. *J. Mol. Biol.* **2005**, *352*, 72−90.
(23) Ghodke, P. P.; Pradeepkumar, P. I. Site-Specific N2-dG DNA Adducts: Formation, Synthesis, and TLS Polymerase-Mediated Bypass. *Eur. J. Org. Chem.* **2020**, *2020*, 6831−6844.
(24) Choi, J.; Guengerich, F. P. Kinetic Evidence for Inefficient and Error-prone Bypass across Bulky N 2 -Guanine DNA Adducts by Human DNA Polymerase i. *J. Biol. Chem.* **2006**, *281*, 12315−12324.
(25) Choi, J.; Angel, K. C.; Guengerich, F. P. Translesion Synthesis across Bulky N 2 -Alkyl Guanine DNA Adducts by Human DNA Polymerase k. *J. Biol. Chem.* **2006**, *281*, 21062−21072.
(26) Yockey, O. P.; Jha, V.; Ghodke, P. P.; Xu, T.; Xu, W.; Ling, H.; Pradeepkumar, P. I.; Zhao, L. Mechanism of Error-Free DNA Replication Past Lucidin-Derived DNA Damage by Human DNA Polymerase κ. *Chem. Res. Toxicol.* **2017**, *30*, 2023−2032.
(27) Choi, J.; Guengerich, F. P. Kinetic Analysis of Translesion Synthesis Opposite Bulky N 2 - and O 6 -Alkylguanine DNA Adducts by Human DNA polymerase REV1. *J. Biol. Chem.* **2008**, *283*, 23645−23655.
(28) Brooks, P. J.; Theruvathu, J. A. DNA adducts from acetaldehyde: implications for alcohol-related carcinogenesis. 2005, *35*, 187−193, DOI: 10.1016/j.alcohol.2005.03.009.
(29) IARC. Tobacco Smoking. In *IARC monographs on the evaluation of carcinogenic risks to humans*; International Agency for Research on Cancer: Lyon, 1986.
(30) IARC. Personal habits and indoor combustions. In *IARC monographs on the evaluation of carcinogenic risks to humans*, vol *100*; International Agency for Research on Cancer: Lyon, 2012.

(31) IARC. Allyl Compounds, Aldehydes, Epoxides and Peroxides. In *IARC monographs on the evaluation of carcinogenic risks to humans*; International Agency for Research on Cancer: Lyon, 1985.
(32) Vaca, C. E.; Fangay, J.; Schwedab, E. K. H. Studies of the reaction of acetaldehyde with deoxynucleosides. *Chem.-Biol. Interact.* **1995**, *98*, 51−67.
(33) Moschel, R. C.; Hudgins, W. R.; Dipple, A. Aralkylation of Guanosine by the Carcinogen N-Nitroso-N-benzylurea. *J. Org. Chem.* **1980**, *45*, 533−535.
(34) Peterson, L. A. N -Nitrosobenzylmethylamine Is Activated to a DNA Benzylating Agent in Rats. *Chem. Res. Toxicol.* **1997**, *10*, 19−26.
(35) Moon, K.-Y.; Kim, Y. S. Synthesis and Characterization of Oligonucleotides Containing Site-Specific Bulky N2-Aralkylated Guanines and N6-Aralkylated Adenines. *Arch. Farm. Res.* **2000**, *23*, 139−146.
(36) Poginsky, B. Formation of genotoxic metabolites from anthraquinone glycosides, present in Rubia tinctorum L. *Mutat. Res.* **1992**, *265*, 263−272.
(37) Bendadani, C.; Meinl, W.; Monien, B. H.; Dobbernack, G.; Glatt, H. The carcinogen 1 - methylpyrene forms benzylic DNA adducts in mouse and rat tissues in vivo via a reactive sulphuric acid ester. *Arch. Toxicol.* **2014**, *88*, 815−821.
(38) Monien, B. H.; Müller, C.; Bakhiya, N.; Donath, C.; Frank, H.; Seidel, A.; Glatt, H. Probenecid, an inhibitor of transmembrane organic anion transporters, alters tissue distribution of DNA adducts in 1-hydroxymethylpyrene-treated rats. *Toxicology* **2009**, *262*, 80−85.
(39) Flesher, J.; Horn, J.; Lehner, A. 9-Sulfooxymethylanthracene is an ultimate electrophilic and carcinogenic form of 9-hydroxymethylanthracene. *Biochem. Biophys. Res. Commun.* **1998**, *251*, 239−243.
(40) Calvo, P. A.; Sastre-Moreno, G.; Perpiñá, C.; Guerra, S.; Martínez-Jiménez, M. I.; Blanco, L. The invariant glutamate of human PrimPol DxE motif is critical for its Mn 2+ −dependent distinctive activities. *DNA Repair* **2019**, *77*, 65−75.
(41) Boldinova, E. O.; Yudkina, A. V.; Shilkin, E. S.; Gagarinskaya, D. I.; Baranovskiy, A. G.; Tahirov, T. H.; Zharkov, D. O.; Makarova, A. V. Translesion activity of PrimPol on DNA with cisplatin and DNA-protein cross-links. *Sci. Rep.* **2021**, *11*, 17588.
(42) Boldinova, E. O.; Manukyan, A. A.; Makarova, A. V. The DNA ligands Arg47 and Arg76 are crucial for catalysis by human PrimPol. *DNA Repair* **2021**, *100*, No. 103048.
(43) Boldinova, E. O.; Stojkovic, G.; Khairullin, R.; Wanrooij, S.; Makarova, A. V. Optimization of the expression, purification and polymerase activity reaction conditions of recombinant human PrimPol. *PLoS One* **2017**, *12*, No. e0184489.
(44) Boldinova, E. O.; Belousova, E. A.; Gagarinskaya, D. I.; Maltseva, E. A.; Khodyreva, S. N.; Lavrik, O. I.; Makarova, A. V. Strand displacement activity of primpol. *Int. J. Mol. Sci.* **2020**, *21*, 9027.
(45) Binz, S. K.; Dickson, A. M.; Haring, S. J.; Wold, M. S. Functional Assays for Replication Protein A (RPA). *Methods Enzymol.* **2006**, *409*, 11−38.
(46) Makarova, A. V.; Stodola, J. L.; Burgers, P. M. J. A four-subunit DNA polymerase ζ complex containing Pol δ accessory subunits is essential for PCNA-mediated mutagenesis. *Nucleic Acids Res.* **2012**, *40*, 11618−11626.
(47) Ghodke, P. P.; Bommisetti, P.; Nair, D. T.; Pradeepkumar, P. I. Synthesis of N2-Deoxyguanosine Modified DNAs and the Studies on Their Translesion Synthesis by the E. coli DNA Polymerase IV. *J. Org. Chem.* **2019**, *84*, 1734−1747.
(48) Rechkoblit, O.; Johnson, R. E.; Gupta, Y. K.; Prakash, L.; Prakash, S.; Aggarwal, A. K. Structural basis of DNA synthesis opposite 8-oxoguanine by human PrimPol primase-polymerase. *Nat. Commun.* **2021**, *12*, 4020.
(49) Vanquelef, E.; Simon, S.; Marquant, G.; Garcia, E.; Klimerak, G.; Delepine, J. C.; Cieplak, P.; Dupradeau, F. Y. R. E. D. Server: A web service for deriving RESP and ESP charges and building force field libraries for new molecules and molecular fragments. *Nucleic Acids Res.* **2011**, *39*, 511−517.
(50) Dupradeau, F. Y.; Pigache, A.; Zaffran, T.; Savineau, C.; Lelong, R.; Grivel, N.; Lelong, D.; Rosanski, W.; Cieplak, P. T. R.E.D. tools: Advances in RESP and ESP charge derivation and force field library building. *Phys. Chem. Chem. Phys.* **2010**, *12*, 7821−7839.
(51) Frisch, M. J.; Trucks, G. W.; Schlegel, H. B.; Scuseria, G. E.; Robb, M. A.; Cheeseman, J. R.; Scalmani, G.; Barone, V.; Petersson, G. A.; Nakatsuji, H. *Gaussian 16, Revision B. 01*; Gaussian, Inc.: Wallingford CT, 2016.
(52) Sali, A.; Blundell, T. L. Comparative protein modelling by satisfaction of spatial restraints. *J. Mol. Biol.* **1993**, *234*, 779−815.
(53) Case, D. A.; Walker, R. C.; Cheatham, T. E.; Simmerling, C.; Roitberg, A.; Merz, K. M.; Luo, R.; Darden, T. *Amber 2018*: Univ. California: San Francisco, 2018.
(54) Maier, J. A.; Martinez, C.; Kasavajhala, K.; Wickstrom, L.; Hauser, K. E.; Simmerling, C. ff14SB: Improving the Accuracy of Protein Side Chain and Backbone Parameters from ff99SB. *J. Chem. Theory Comput.* **2015**, *11*, 3696−3713.
(55) Galindo-Murillo, R.; Robertson, J. C.; Zgarbová, M.; Šponer, J.; Otyepka, M.; Jurečka, P.; Cheatham, T. E. Assessing the Current State of Amber Force Field Modifications for DNA. *J. Chem. Theory Comput.* **2016**, *12*, 4114−4127.
(56) Götz, A. W.; Williamson, M. J.; Xu, D.; Poole, D.; Le Grand, S.; Walker, R. C. Routine microsecond molecular dynamics simulations with AMBER on GPUs. 1. generalized born. *J. Chem. Theory Comput.* **2012**, *8*, 1542−1555.
(57) Salomon-Ferrer, R.; Götz, A. W.; Poole, D.; Le Grand, S.; Walker, R. C. Routine microsecond molecular dynamics simulations with AMBER on GPUs. 2. Explicit solvent particle mesh ewald. *J. Chem. Theory Comput.* **2013**, *9*, 3878−3888.
(58) Roe, D. R.; Cheatham, T. E. PTRAJ and CPPTRAJ: Software for processing and analysis of molecular dynamics trajectory data. *J. Chem. Theory Comput.* **2013**, *9*, 3084−3095.
(59) Wan, L.; Lou, J.; Xia, Y.; Su, B.; Liu, T.; Cui, J.; Sun, Y.; Lou, H.; Huang, J. HPrimpol1/CCDC111 is a human DNA primase-polymerase required for the maintenance of genome integrity. *EMBO Rep.* **2013**, *14*, 1104−1112.
(60) Martínez-Jiménez, M. I.; Lahera, A.; Blanco, L. Human PrimPol activity is enhanced by RPA. *Sci. Rep.* **2017**, *7*, 783.
(61) Guilliam, T. A.; Bailey, L. J.; Brissett, N. C.; Doherty, A. J. PolDIP2 interacts with human PrimPol and enhances its DNA polymerase activities. *Nucleic Acids Res.* **2016**, *44*, 3317−3329.
(62) Makarova, A. V.; Burgers, P. M. J. Eukaryotic DNA polymerase ζ. *DNA Repair* **2015**, *29*, 47−55.
(63) Kathuria, P.; Singh, P.; Sharma, P.; Wetmore, S. D. Replication of the Aristolochic Acid I Adenine Adduct (ALI-N6-A) by a Model Translesion Synthesis DNA Polymerase: Structural Insights on the Induction of Transversion Mutations from Molecular Dynamics Simulations. *Chem. Res. Toxicol.* **2020**, *33*, 2573−2583.
(64) Royer, W. E.; Pardananii, A.; Gibson, Q. H.; Peterson, E. S.; Friedman, J. M. Ordered water molecules as key allosteric mediators in a cooperative dimeric hemoglobin. *Proc. Natl. Acad. Sci. U. S. A.* **1996**, *93*, 14526−14531.
(65) Knight, J. D. R.; Hamelberg, D.; McCammon, J. A.; Kothary, R. The role of conserved water molecules in the catalytic domain of protein kinases. *Proteins* **2009**, *76*, 527−535.
(66) Rechkoblit, O.; Gupta, Y. K.; Malik, R.; Rajashankar, K. R.; Johnson, R. E.; Prakash, L.; Prakash, S.; Aggarwal, A. K. Structure and mechanism of human PrimPol, a DNA polymerase with primase activity. *Sci. Adv.* **2016**, *2*, No. e1601317.
(67) Zafar, M. K.; Ketkar, A.; Lodeiro, M. F.; Cameron, C. E.; Eoff, R. L. Kinetic analysis of human PrimPol DNA polymerase activity reveals a generally error-prone enzyme capable of accurately bypassing 7,8-dihydro-8-oxo-2′-deoxyguanosine. *Biochemistry* **2014**, *53*, 6584−6594.
(68) Brooks, P. J.; Zakhari, S. Acetaldehyde and the Genome: Beyond Nuclear DNA Adducts and Carcinogenesis. *Environ. Mol. Mutagen.* **2014**, *91*, 77−91.
(69) Upton, D. C.; Wang, X.; Blans, P.; Perrino, F. W.; Fishbein, J. C.; Akman, S. A. Replication of N2-ethyldeoxyguanosine DNA

https://doi.org/10.1021/acschembio.2c00717
ACS Chem. Biol. 2022, 17, 3238−3250

adducts in the human embryonic kidney cell line 293. *Chem. Res. Toxicol.* **2006**, *19*, 960−967.
(70) Pence, M. G.; Blans, P.; Zink, C. N.; Hollis, T.; Fishbein, J. C.; Perrino, F. W. Lesion Bypass of N 2 -Ethylguanine by Human DNA polymerase iota. *J. Biol. Chem.* **2009**, *284*, 1732−1740.
(71) Pence, M. G.; Blans, P.; Zink, C. N.; Fishbein, J. C.; Perrino, F. W. Bypass of N 2 -ethylguanine by human DNA polymerase k. *DNA Repair* **2011**, *10*, 56−64.
(72) Tokarsky, E. J.; Wallenmeyer, P. C.; Phi, K. K.; Suo, Z. Significant impact of divalent metal ions on the fidelity, sugar selectivity, and drug incorporation efficiency of human PrimPol. *DNA Repair* **2016**, *49*, 51−59.
(73) Washington, M. T.; Minko, I. G.; Johnson, R. E.; Haracska, L.; Harris, T. M.; Lloyd, R. S.; Prakash, S.; Prakash, L. Efficient and Error-Free Replication past a Minor-Groove N2 -Guanine Adduct by the Sequential Action of Yeast Rev1 and DNA Polymerase zeta. *Mol. Cell. Biol.* **2004**, *24*, 6900−6906.
(74) Rodr, A.; Liu, Z.; Lin, C. H.; Ding, S.; Cai, Y.; Kolbanovskiy, A.; Kolbanovskiy, M.; Amin, S.; Broyde, S.; Geacintov, N. E. Nuclear Magnetic Resonance Studies of an N2-Guanine Adduct Derived from the Tumorigen Dibenzo[a,l]pyrene in DNA: Impact of Adduct Stereochemistry, Size, and Local DNA Sequence on Solution Conformations. *Biochemistry* **2014**, *53*, 1827−1841.
(75) Minko, I. G.; Washington, M. T.; Prakash, L.; Prakash, S.; Lloyd, R. S. Translesion DNA Synthesis by Yeast DNA Polymerase eta on Templates Containing N2-Guanine Adducts of 1,3-Butadiene Metabolites. *J. Biol. Chem.* **2001**, *276*, 2517−2522.
(76) Blackwell, L. J.; Borowiec, J. A. Human Replication Protein A Binds Single-Stranded DNA in Two Distinct Complexes. *Mol. Cell. Biol.* **1994**, *14*, 3993−4001.
(77) Kim, C.; Paulus, B. F.; Wold, M. S. Interactions of Human Replication Protein A with Oligonucleotides. *Biochemistry* **1994**, *33*, 14197−14206.
(78) Bochkarev, A.; Pfuetzner, R. A.; Edwards, A. M.; Frappier, L. Structure of the single- domain of replication protein A bound to DNA. *Nature* **1997**, *385*, 176−181.
(79) Krasikova, Y. S.; Rechkunova, N. I.; Maltseva, E. A.; Lavrik, O. I. RPA and XPA interaction with DNA structures mimicking intermediates of the late stages in nucleotide excision repair. *PLoS One* **2018**, *13*, No. e0190782.

https://doi.org/10.1021/acschembio.2c00717
ACS Chem. Biol. 2022, 17, 3238−3250

Supporting Information

Translesion synthesis across N^2-ethyl-deoxyguanosine adduct by human PrimPol

Elizaveta O. Boldinova[1#], Pratibha P. Ghodke[2#], Sruthi Sudhakar[2#], Vipin Kumar Mishra[2], Anna A. Manukyan[1], Nataliya Miropolskaya[1], Pushpangadan I. Pradeepkumar[2]*, Alena V. Makarova[1]*

[1] *Institute of Molecular Genetics, National Research Center «Kurchatov Institute», Kurchatov sq. 2, 123182, Moscow, Russia*
[2] *Department of Chemistry, Indian Institute of Technology Bombay, Powai, Mumbai, 400076, India*

[#] equal contribution
* corresponding authors
E-mail address: amakarova-img@yandex.ru (A.V. Makarova); pradeep@chem.iitb.ac.in (P.I. Pradeepkumar).

Cartesian coordinates and RESP charges of the N^2-Et-dG nucleotide

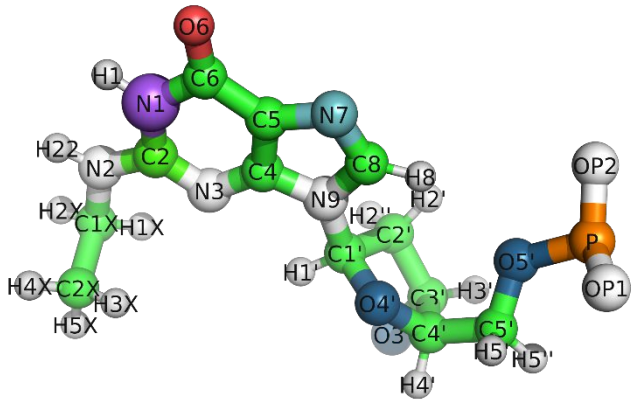

@<TRIPOS>MOLECULE
ET
39 41 1 0 1
SMALL
USER_CHARGES
@<TRIPOS>ATOM

1	O5'	-2.681216	0.861873	-0.510199	OS	1	ET	-0.4899
2	P	-4.119164	0.974638	-1.294949	P	1	ET	1.2125
3	OP1	-4.401945	2.394020	-1.554208	O2	1	ET	-0.7918
4	OP2	-5.033915	0.046113	-0.614584	O2	1	ET	-0.7918
5	O3'	1.407593	0.000000	0.000000	OS	1	ET	-0.5217
6	C5'	-1.668934	1.759010	-0.843942	CI	1	ET	-0.0361
7	H5'	-1.980550	2.782268	-0.659163	H1	1	ET	0.0821
8	H5''	-1.403925	1.665423	-1.895223	H1	1	ET	0.0821
9	C4'	-0.444371	1.469428	0.000000	CT	1	ET	0.1835
10	H4'	0.372963	2.083461	-0.357778	H1	1	ET	0.1058
11	O4'	-0.710373	1.803581	1.345348	OS	1	ET	-0.3956
12	C1'	-0.494626	0.721162	2.205330	CT	1	ET	0.1366
13	H1'	0.470708	0.806768	2.680151	H2	1	ET	0.1299
14	N9	-1.474549	0.760952	3.260351	N*	1	ET	0.035
15	C8	-2.841424	0.875814	3.119091	CK	1	ET	0.108
16	H8	-3.285590	0.940074	2.148660	H5	1	ET	0.1833
17	N7	-3.463174	0.909682	4.235075	NB	1	ET	-0.5625
18	C5	-2.472973	0.818401	5.189299	CB	1	ET	0.1509
19	C6	-2.550310	0.801732	6.620951	C	1	ET	0.5405
20	O6	-3.487699	0.852519	7.360539	O	1	ET	-0.5536
21	N1	-1.249552	0.701469	7.169240	NA	1	ET	-0.4973
22	H1	-1.239107	0.640244	8.164713	H	1	ET	0.3193
23	C2	-0.081113	0.621397	6.473317	CA	1	ET	0.5977
24	N2	1.043079	0.496404	7.216719	N2	1	ET	-0.7036
25	H22	0.970306	0.727599	8.181593	H	1	ET	0.3975
26	N3	-0.023943	0.635782	5.182918	NC	1	ET	-0.4764
27	C4	-1.242871	0.732380	4.596914	CB	1	ET	0.1241
28	C3'	0.000000	0.000000	0.000000	CT	1	ET	0.0594

29	H3'	-0.379612	-0.537641	-0.861178	H1	1	ET	0.1138
30	C2'	-0.570497	-0.517706	1.313794	CT	1	ET	-0.0979
31	H2'	-1.601010	-0.816898	1.179538	HC	1	ET	0.0572
32	H2"	-0.012541	-1.352651	1.721971	HC	1	ET	0.0572
33	C1X	2.375625	0.551277	6.635261	CT	1	ET	0.1854
34	H1X	2.359479	-0.028112	5.725087	H1	1	ET	0.0292
35	H2X	3.039024	0.049384	7.329913	H1	1	ET	0.0292
36	C2X	2.869149	1.967825	6.358039	CT	1	ET	-0.0842
37	H3X	2.222094	2.466797	5.647121	HC	1	ET	0.0274
38	H4X	2.898983	2.557268	7.269920	HC	1	ET	0.0274
39	H5X	3.872956	1.940749	5.945084	HC	1	ET	0.0274

@<TRIPOS>BOND

1	1	2	1
2	1	6	1
3	2	3	1
4	2	4	1
5	5	28	1
6	6	7	1
7	6	8	1
8	6	9	1
9	9	10	1
10	9	11	1
11	9	28	1
12	11	12	1
13	12	13	1
14	12	14	1
15	12	30	1
16	14	15	1
17	14	27	1
18	15	16	1
19	15	17	1
20	17	18	1
21	18	19	1
22	18	27	1
23	19	20	1
24	19	21	1
25	21	22	1
26	21	23	1
27	23	24	1
28	23	26	1
29	24	25	1
30	24	33	1
31	26	27	1
32	28	29	1
33	28	30	1
34	30	31	1
35	30	32	1
36	33	34	1
37	33	35	1

```
    38        33          36          1
    39        36          37          1
    40        36          38          1
    41        36          39          1
      @<TRIPOS>SUBSTRUCTURE
 1          MOL          1          ****          0          ****          ****
```

Figure S1. Cartesian coordinates and RESP charges of the N^2-Et-dG nucleotide. The Cartesian coordinates and RESP charges of N^2-Et-dG nucleotide derived from the RED server using previously established protocols. A theory level of HF/6-31G* was used for the calculations. Detailed procedure for the derivation of partial charges for modified nucleotide fragments can be found in the tutorial at: http://upjv.q4md-forcefieldtools.org/Tutorial/Tutorial-4.php

Cartesian coordinates and RESP charges of the N^2-Ib-dG nucleotide

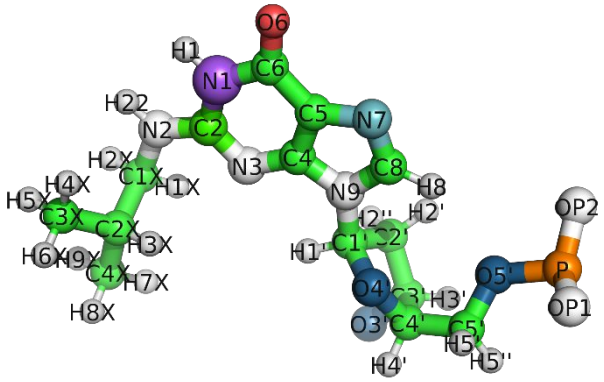


```
@<TRIPOS>MOLECULE
IB
          45           47            1            0  1
 SMALL
 USER_CHARGES
 @<TRIPOS>ATOM
      1  O5'       -2.680995     0.861036    -0.511117  OS        1  IB          -0.4861
      2  P         -4.118742     0.973449    -1.296284  P         1  IB           1.2119
      3  OP1       -4.402051     2.392797    -1.555153  O2        1  IB          -0.792
      4  OP2       -5.033310     0.044301    -0.616523  O2        1  IB          -0.792
      5  O3'        1.407669     0.000000     0.000000  OS        1  IB          -0.5166
      6  C5'       -1.668993     1.758720    -0.844235  CI        1  IB          -0.0334
      7  H5'       -1.981068     2.781785    -0.659168  H1        1  IB           0.0866
      8  H5"       -1.403665     1.665619    -1.895488  H1        1  IB           0.0866
      9  C4'       -0.444555     1.469386     0.000000  CT        1  IB           0.1273
     10  H4'        0.372759     2.083529    -0.357695  H1        1  IB           0.1218
     11  O4'       -0.710940     1.803475     1.345203  OS        1  IB          -0.3793
     12  C1'       -0.494643     0.721152     2.205361  CT        1  IB           0.1582
     13  H1'        0.470880     0.807103     2.679719  H2        1  IB           0.1217
     14  N9        -1.473855     0.760625     3.260763  N*        1  IB           0.0011
     15  C8        -2.841222     0.873678     3.120315  CK        1  IB           0.1185
```

16	H8	-3.286110	0.936418	2.150104	H5	1	IB	0.1797
17	N7	-3.462088	0.907962	4.236576	NB	1	IB	-0.5573
18	C5	-2.470967	0.818704	5.190362	CB	1	IB	0.1243
19	C6	-2.546918	0.805617	6.621783	C	1	IB	0.5588
20	O6	-3.483296	0.859248	7.362636	O	1	IB	-0.5575
21	N1	-1.245650	0.706916	7.169439	NA	1	IB	-0.5284
22	H1	-1.234702	0.663718	8.165796	H	1	IB	0.3292
23	C2	-0.076980	0.627593	6.473009	CA	1	IB	0.6119
24	N2	1.047400	0.515318	7.212237	N2	1	IB	-0.6227
25	H22	0.969476	0.655497	8.192605	H	1	IB	0.3667
26	N3	-0.021621	0.638180	5.181442	NC	1	IB	-0.5097
27	C4	-1.240903	0.733907	4.597206	CB	1	IB	0.1631
28	C3'	0.000000	0.000000	0.000000	CT	1	IB	0.0562
29	H3'	-0.379512	-0.537654	-0.861208	H1	1	IB	0.1173
30	C2'	-0.570409	-0.517720	1.313801	CT	1	IB	-0.1137
31	H2'	-1.600890	-0.817035	1.179582	HC	1	IB	0.0653
32	H2"	-0.012351	-1.352617	1.721957	HC	1	IB	0.0653
33	C1X	2.381406	0.512107	6.635403	CT	1	IB	0.0044
34	H1X	2.347611	-0.089780	5.739386	H1	1	IB	0.0594
35	H2X	3.027986	0.005619	7.345155	H1	1	IB	0.0594
36	C2X	2.948331	1.900200	6.312462	CT	1	IB	0.2256
37	H3X	2.256062	2.382489	5.629164	HC	1	IB	0.0018
38	C3X	3.082585	2.770238	7.564767	CT	1	IB	-0.1801
39	H4X	2.125327	2.925966	8.052400	HC	1	IB	0.0378
40	H5X	3.759600	2.317612	8.286334	HC	1	IB	0.0378
41	H6X	3.478001	3.749167	7.313810	HC	1	IB	0.0378
42	C4X	4.296959	1.748554	5.603649	CT	1	IB	-0.1801
43	H7X	4.200881	1.167316	4.691588	HC	1	IB	0.0378
44	H8X	4.705085	2.717553	5.335535	HC	1	IB	0.0378
45	H9X	5.023518	1.250925	6.241916	HC	1	IB	0.0378

@<TRIPOS>BOND

1	1	2	1
2	1	6	1
3	2	3	1
4	2	4	1
5	5	28	1
6	6	7	1
7	6	8	1
8	6	9	1
9	9	10	1
10	9	11	1
11	9	28	1
12	11	12	1
13	12	13	1
14	12	14	1
15	12	30	1
16	14	15	1
17	14	27	1
18	15	16	1

```
     19        15        17        1
     20        17        18        1
     21        18        19        1
     22        18        27        1
     23        19        20        1
     24        19        21        1
     25        21        22        1
     26        21        23        1
     27        23        24        1
     28        23        26        1
     29        24        25        1
     30        24        33        1
     31        26        27        1
     32        28        29        1
     33        28        30        1
     34        30        31        1
     35        30        32        1
     36        33        34        1
     37        33        35        1
     38        33        36        1
     39        36        37        1
     40        36        38        1
     41        36        42        1
     42        38        39        1
     43        38        40        1
     44        38        41        1
     45        42        43        1
     46        42        44        1
     47        42        45        1
       @<TRIPOS>SUBSTRUCTURE
1          MOL          1          ****          0          ****          ****
```

Figure S2. Cartesian coordinates and RESP charges of the N^2-Ib-dG nucleotide. The Cartesian coordinates and RESP charges of N^2-Ib-dG nucleotide derived from the RED server using previously established protocols. A theory level of HF/6-31G* was used for the calculations. Detailed procedure for the derivation of partial charges for modified nucleotide fragments can be found in the tutorial at: http://upjv.q4md-forcefieldtools.org/Tutorial/Tutorial-4.php

TLS activity of PrimPol and Pol ζ$_4$ on DNA with N^2-Et-dG

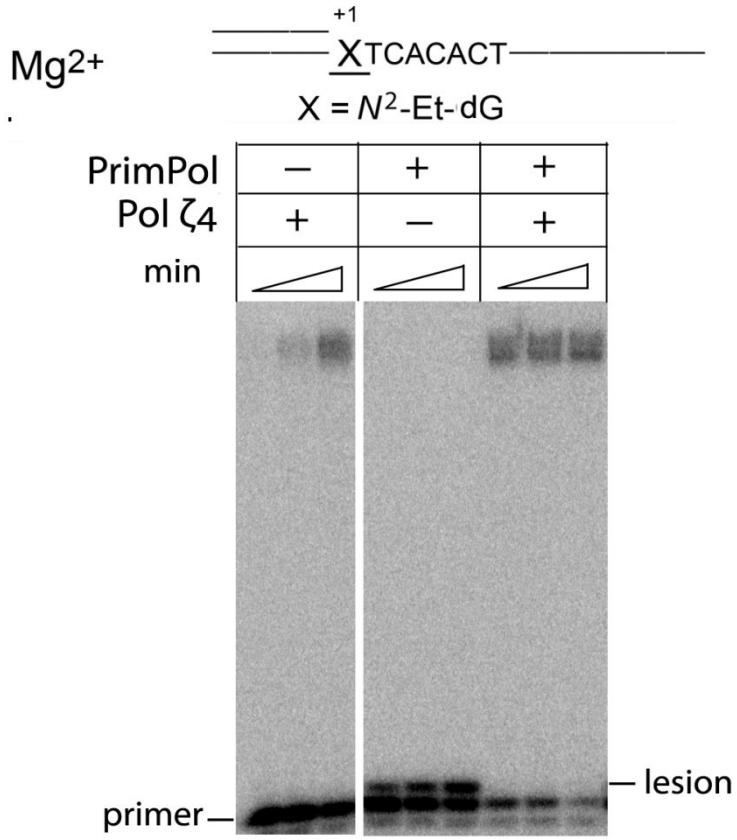

Figure S3. The TLS activity of PrimPol and Pol ζ$_4$ on DNA substrate with N^2-Et-dG. The standing start primer extension reactions with 400 nM PrimPol and 30 nM Pol ζ$_4$ in the presence of Mn^{2+} ions and dNTPs for 5, 10 or 20 min.

RMSD of the c-α atoms of the various N^2-dG complexes

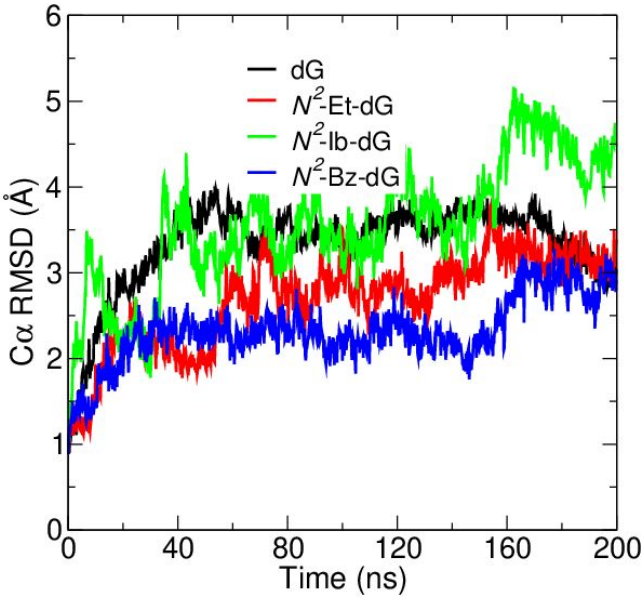

Figure S4. RMSD of the c-α atoms of the various N^2-dG complexes. The root mean square deviation of the c-alpha atoms of PrimPol across various N^2-dG complexes was calculated from the 200 ns trajectory. The RMSD is plotted as a function of time.

Representative images showing reorientation of adducts and altering reaction parameters

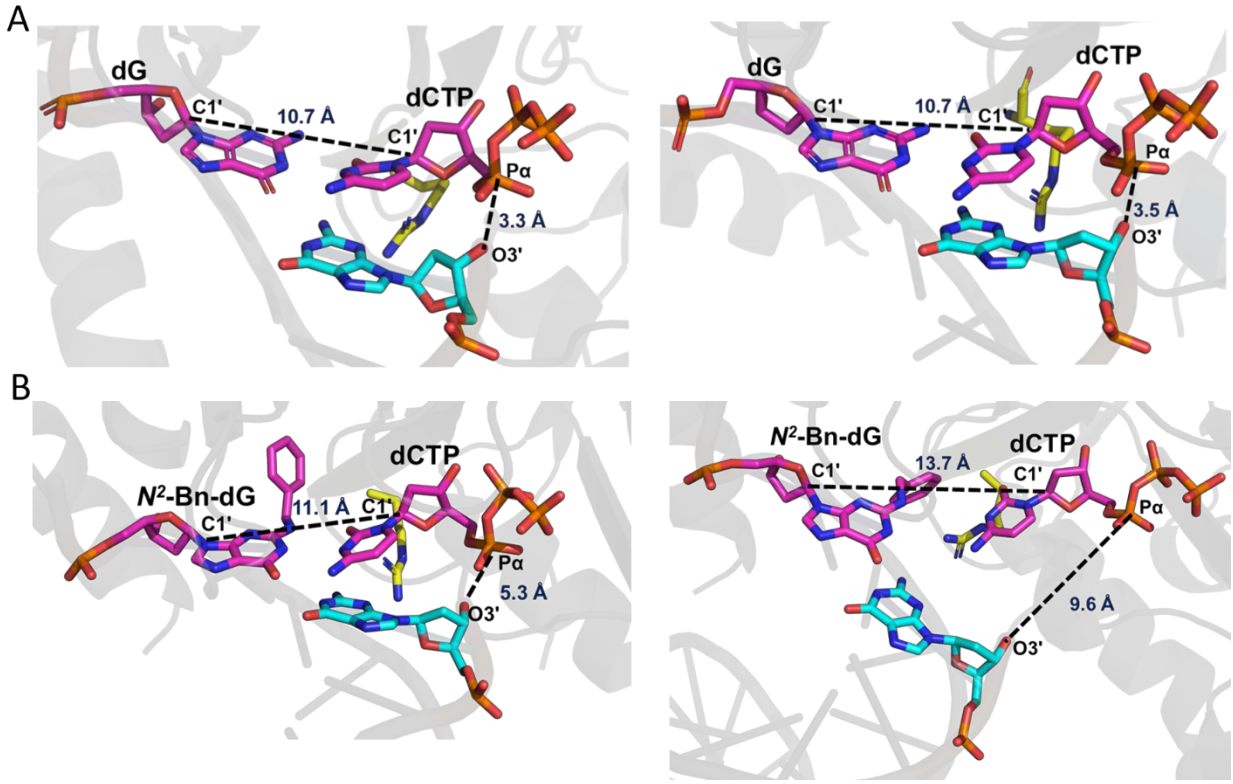

Figure S5. (A) Representative images showing the unmodified N^2-dG complex in the beginning and a mid-frame of the simulation; (B) Representative images showing the unmodified N^2-Bn-dG complex in the beginning and a mid-frame of the simulation. The reaction distance and C1′- C1′ distances are represented in black dashed lines. The reorientation in the N^2-Bn-dG complex and the changes in structural parameters are visible.

Structural parameters for the successful replication in the simulations with Mn^{2+} ions

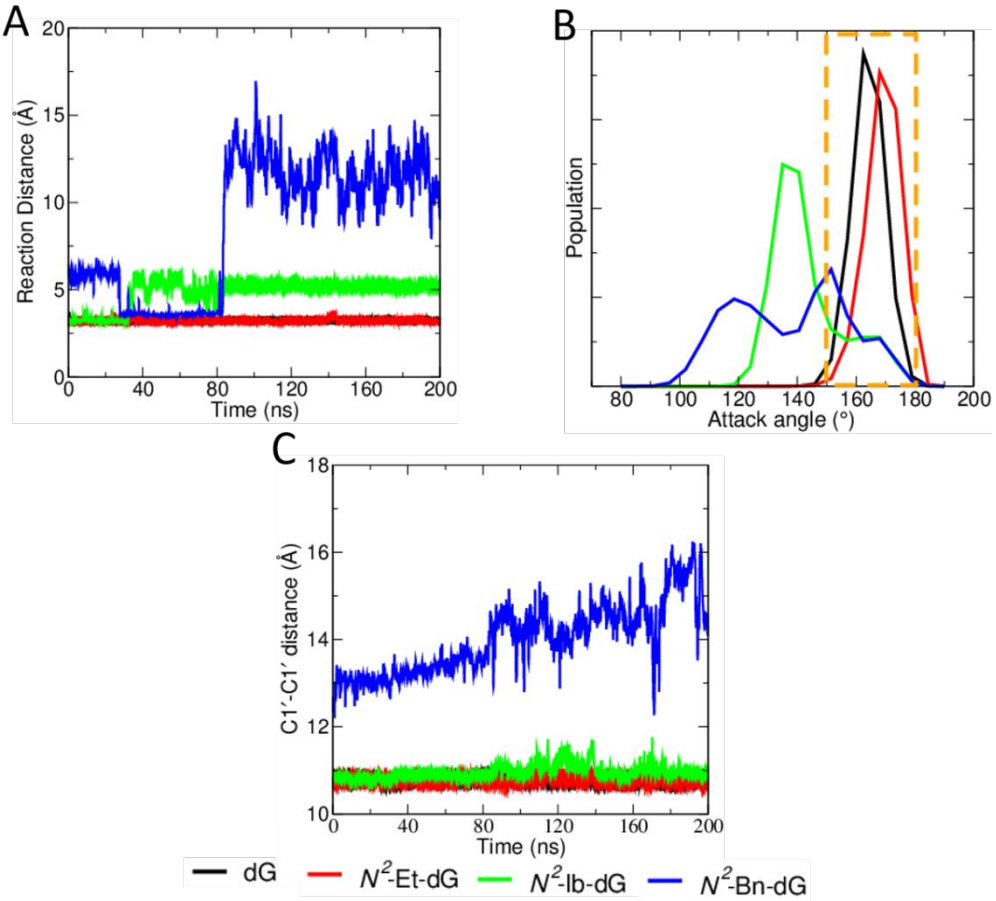

Figure S6. The structural parameters associated with the insertion stage of the PrimPol in the presence of Mn^{2+} ions. (A) The reaction distance calculated between the O3′ of the primer strand and the Pα of dCTP; (B) The attack angle calculated between the O3′ of the primer strand and the Pα, Oαβ of dCTP; (C) The C1′- C1′ distance between the adduct and dCTP for the various complexes.

The total number of water molecules around the metal cofactors

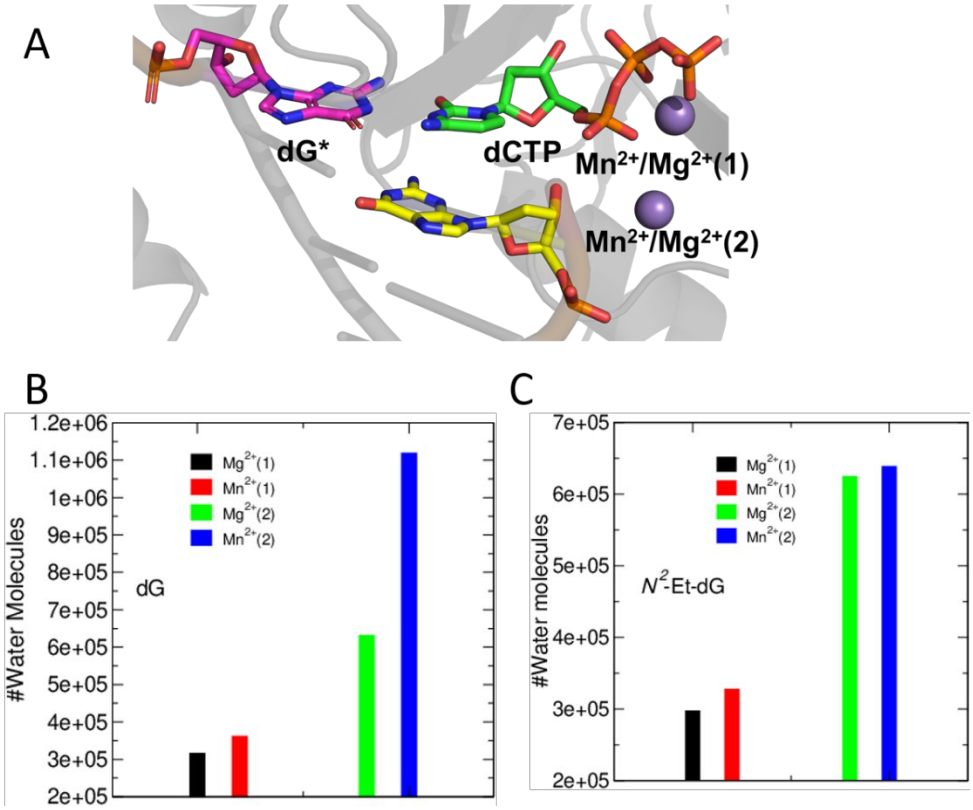

Figure S7. (A) Representative image of the N^2-dG complex with the first and second Mn^{2+}/Mg^{2+} ions numbered; (B) The total number of water molecules in the 5 Å cut off around the metal cofactors in dG complex; and (C) The total number of water molecules in the 5 Å cut off around, the metal cofactors in N^2-Et-dG complex.

TLS activity of PrimPol mutants on DNA substrates with dG and N^2-Et-dG

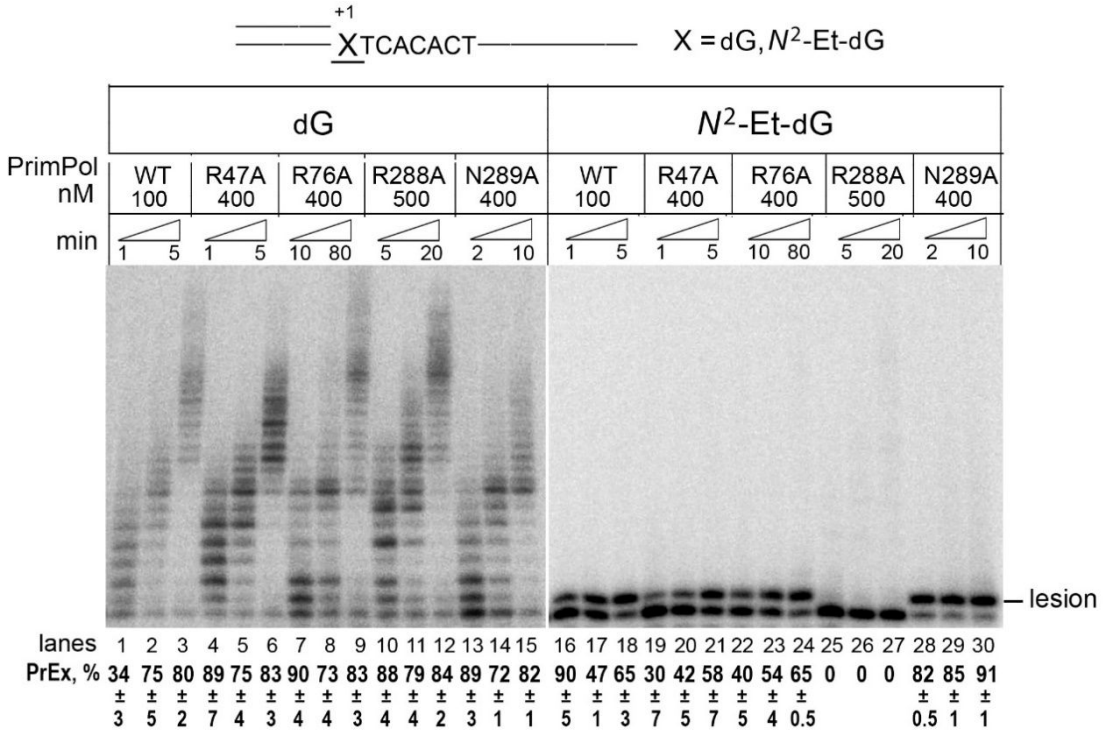

Figure S8. The TLS activity of PrimPol variants with R47A, R76A, R288A and N289A substitutions on DNA substrates with dG and N^2-Et-dG. The standing start primer extension reactions with 100 nM wild-type PrimPol, 400 nM R47A, R46A and N289A variants, and 500 nM R288A mutant variant in the presence of Mn^{2+} ions and dNTPs for different times as indicated.

Population distribution of H-bond count between dCTP and the protein network in N^2-dG complexes

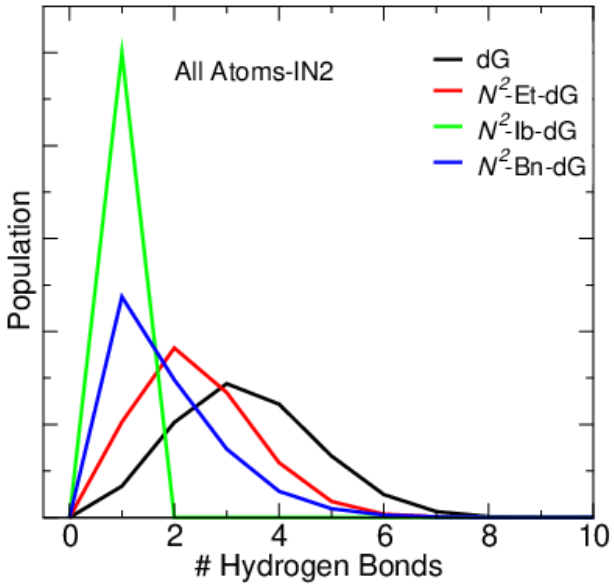

Figure S9. The population distribution of H-bond counts between the dCTP and protein network within 5 Å in various N^2-dG complexes.

Reorientation of catalytic amino acids, adducts and incoming nucleotide in N^2-Ib-dG and N^2-Bn-dG complexes during the simulation

A

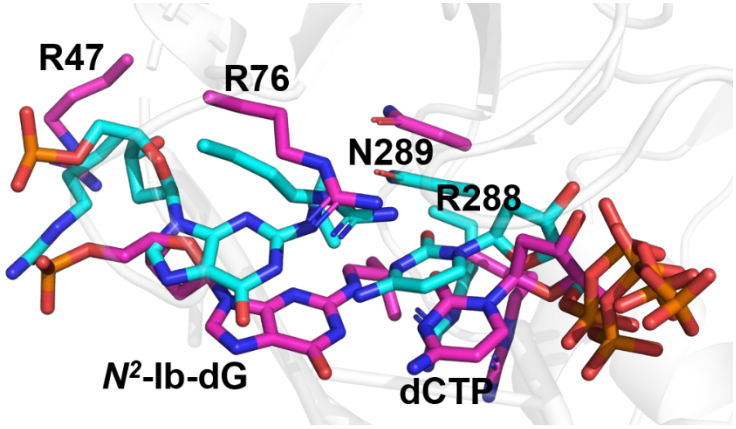

B

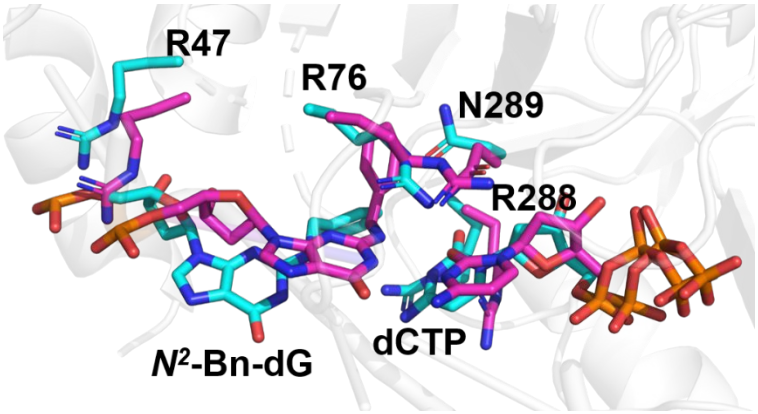

Figure S10. The reorientation of the catalytic amino acid residues, adducts, and the incoming nucleotide in (A) N^2-Ib-dG and (B) N^2-Bn-dG complexes during the 200 ns simulation. The magenta color represents the initial simulation frame, and the cyan color represents the frame after 100 ns. The background amino acids are made transparent for clarity.

Table S1. The Hydrogen bond occupancy between the DNA adduct and dCTP

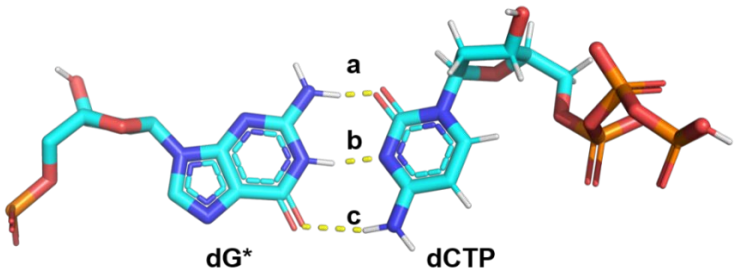

Adduct	% of H-Bond a	% of H-Bond b	% of H-Bond c
dG	99.4	99.7	94.1
N^2-Et-dG	95.7	98.2	96.2
N^2-Ib-dG	27.2	38.8	30.0
N^2-Bn-dG	4.8	6.5	7.3
The H-bond occupancies between the N^2-dG adduct and incoming nucleotide calculated from the 200 ns MD trajectories. The H-bond was calculated with a distance cut-off of 3.5 Å and an angle cut-off of 135 degrees.			

Table S2. The role of the conservative active site residues contacting an incoming nucleotide and the template base

Amino acid residue	Possible role	reference
Arg47	Mutation R47A affects the dNMPs incorporation opposite undamaged DNA, 8-oxo-G and an 1,2-intrastrand cisplatin cross-link	1, 2
Arg76	Mutation R76A affects the dNMPs incorporation opposite undamaged DNA, 8-oxo-G and an 1,2-intrastrand cisplatin cross-link	1, 2
	The side chain of Arg76 collides with the 5′ base of the (6–4) T-T dimer, possibly affecting the accommodation of distorting DNA lesions	3
Asn289	The backbone carboxyl oxygen of Asn289 sterically clashes with the ribose 2′-hydroxyl of incoming nucleotide possibly playing a role in the discrimination of ribonucleotides	3

References

1. Boldinova, E. O., Yudkina, A. V., Shilkin, E. S., Gagarinskaya, D. I., Baranovskiy, A. G., Tahirov, T. H., Zharkov, D. O. & Makarova, A. V. Translesion activity of PrimPol on DNA with cisplatin and DNA-protein cross-links. *Sci. Rep.* **2021,** *11*, 17588.
2. Boldinova, E. O., Manukyan, A. A. & Makarova, A. V. The DNA ligands Arg47 and Arg76 are crucial for catalysis by human PrimPol. *DNA Repair (Amst).* **2021,** *100*, 103048.
3. Rechkoblit, O., Gupta, Y. K., Malik, R., Rajashankar, K. R., Johnson, R. E., Prakash, L., Prakash, S. & Aggarwal, A. K. Structure and mechanism of human PrimPol, a DNA polymerase with primase activity. *Sci. Adv.* **2016,** *2*, e1601317.